

# Modeling the spatially distributed nature of subglacial sediment transport and erosion

Ian Delaney<sup>1</sup>, Leif Anderson<sup>1,2</sup>, and Frédéric Herman<sup>1</sup>

<sup>1</sup>Institut des dynamiques de la surface terrestre (IDYST), Université de Lausanne, Bâtiment Géopolis, CH-1015 Lausanne

<sup>2</sup>Department of Geology and Geophysics, University of Utah, Frederick Albert Sutton Building, 115 S 1460 E, Salt Lake City, UT 84112-0102, USA

**Correspondence:** Ian Delaney (IanArburua.Delaney@unil.ch)

**Abstract.** In addition to ice and water, glaciers expel sediment. As a result, changing glacier dynamics and melt ~~will~~ result in changes to glacier erosion and sediment discharge, which can impact the landscape surrounding retreating glaciers, as well as communities and ecosystems downstream. To date, ~~the available models of subglacial sediment transport on the available models that transport subglacial sediment on~~ sub-hourly to decadal ~~scale transport sediment scales are~~ in one dimension, usually along a glacier's flow line. Such models have proven useful in describing the formation of landforms, the impact of sediment transport on glacier dynamics, ~~the interactions between and the interactions among~~ climate, glacier dynamics, and erosion. However, ~~in one dimension,~~ these models omit the ~~two-dimensional two-dimensional~~ spatial distribution of sediment and its impact on sediment connectivity, *i.e.* the movement of sediment between its detachment in source areas and its deposition in sinks. In turn, ~~the geoscience community needs there is a need for~~ modeling frameworks that describe subglacial sediment discharge in two spatial dimensions ( $x$  and  $y$ ) over time. Here, we present SUGSET\_2D, a numerical model that evolves a two-dimensional subglacial till layer in response to ~~the erosion of bedrock bedrock erosion~~ and changing sediment transport conditions below glaciers. Experiments performed using an idealized alpine glacier ~~demonstrate illustrate~~ the heterogeneity in sediment transport and bedrock erosion below glaciers. The experiments show ~~a non-linear an~~ increase in sediment discharge following increased glacier melt, ~~as has been documented in field observations and other numerical experiments~~. We also apply the model to a real alpine glacier. ~~We compare simulations Model outputs are compared~~ with annual observations of sediment discharge measured from Griesgletscher in the Swiss Alps. SUGSET\_2D reproduces ~~general quantities of sediment discharge and~~ the year-to-year sediment discharge pattern measured at the glacier terminus. The model's ability to match the data depends greatly on the sediment grain size parameter, which controls subglacial sediment transport capacity. Smaller grain sizes allow sediment transport to occur in regions of the bed with reduced water flow and channel size, effectively increasing sediment connectivity into the main channels. Model outputs from both cases show the importance of considering ~~spatial~~ heterogeneities in water discharge and sediment transport in both the  ~~$x$ —and  $y$ —dimensions  $x$ - and  $y$ - dimensions in evaluating sediment discharge from glaciers~~.

## 1 Introduction

Increasing glacier ablation perturbs the ways that glaciers erode bedrock and supply sediment downstream (e.g. Church and Ryder, 1972; Lane et al., 2017; Delaney and Adhikari, 2020). Changing sediment discharge from glaciers in alpine and polar landscapes impacts many downstream social and earth systems (Milner et al., 2017; Li et al., 2021). In turn, predictive models are needed to understand the response of these systems to glacier retreat. In alpine environments, increased sediment discharge leads to the more rapid filling of proglacial reservoirs (Thapa et al., 2005) and the abraiding of hydropower infrastructure (e.g. Felix et al., 2016). The flux of sediment from glaciers also dramatically alters alpine ecosystems (Milner et al., 2017). In the Arctic, increased sediment discharge can affect biogeochemical cycles given that sediments may carry phosphorus and iron (Bhatia et al., 2013; Hawkings et al., 2014). These elements are limiting nutrients in the oceanic ecosystem, so any change to sediment discharge from the ice sheet can alter Arctic ecosystems (Wadham et al., 2019). Modeling studies and observations suggest that increases in sediment output from alpine glaciers could occur when high melt extends up-glacier, mobilizing sediment in new areas (Lane et al., 2017; Delaney and Adhikari, 2020; Li et al., 2021).

Generally, two processes determine the sediment discharge below glaciers: one process adds sediment, the other removes sediment from subglacial till layers (Figure 1; Brinkerhoff et al., 2017; Delaney et al., 2019). Bedrock erosion adds material to the subglacial till layer. Bedrock erosion is accomplished by quarrying, when pressure differentials on opposing sides of obstacles cause fractures to expand and rock to detach (Iverson, 1990; Alley et al., 1997; Hallet et al., 1996; Iverson, 2012), and abrasion, when debris embedded in the ice grinds bedrock as the glacier slides above (Hallet, 1979; Alley et al., 1997). Representing these physical processes in models requires independent knowledge of a large number of parameters (c.f. Ugelvig et al., 2018), so many researchers use empirical relationships that relate glacier sliding to glacier erosion (Humphrey and Raymond, 1994; Koppes et al., 2015; Herman et al., 2015; Cook et al., 2020). The sliding relationship with glacier erosion proves especially useful when applied over large temporal and spatial scales, to explore the coupling between glacier erosion of glacier erosion, climate, and tectonic uplift (e.g. Egholm et al., 2009; Prasicek et al., 2018; Herman et al., 2018; Prasicek et al., 2020; Seguinot et al., 2021).

Conversely, fluvial sediment transport removes mobilizes material from subglacial till layers (e.g. Walder and Fowler, 1994; Ng, 2000; Creyts et al., 2013), or may deposit it there (e.g. Beaud et al., 2018b) under certain hydraulic conditions (e.g. Beaud et al., 2018b). When subglacial water velocity increases above a critical threshold, sediment of a given grain size is transported downvalley downglacier, and if the water velocity slows below the threshold, sediment may be deposited (Shields, 1936). The sediment mobilization ceases when no sediment is present, and the system is supply-limited (e.g. Mao et al., 2014) (e.g. Mao et al., 2014). It follows that fluvial sediment transport depends both on both the subglacial hydraulic characteristics (e.g. Walder and Fowler, 1994), as well as the (e.g. Walder and Fowler, 1994), and the the availability of sediment at the glacier bed (e.g. Willis et al., 1996; Swift et al., 2005) (e.g. Willis et al., 1996; Swift et al., 2005).

Bedrock erosion and fluvial sediment transport vary depending on the characteristics of each glacier. Bedrock erosion tends to dominate sediment transport-discharge below glaciers with minimal sediment storage, large concentrations

of subglacial debris entrained at the glacier ~~sole-bed~~ and steep gradients (Hallet, 1979; Humphrey and Raymond, 1994; Herman et al., 2015; Ugelvig et al., 2018; Herman et al., 2021). Landscape evolution models that represent glacier landscapes ~~demonstrate-illustrate~~ the dominant role of erosional processes, as opposed to sediment transport processes, over geologic timescales (Harbor et al., 1988; Herman et al., 2011; Egholm et al., 2012). Over shorter timescales of months to decades fluvial sediment transport often drives sediment discharge from glaciers (~~e.g. Delaney et al., 2018b; Perolo et al., 2018; Delaney et al., 2019~~) (e.g., Delaney et al., 2018b; Perolo et al., 2018; Delaney et al., 2019).

The development of numerical models of subglacial sediment transport ~~have-has~~ thus far focused on processes acting a single downglacier (~~x-e.g., x-~~) dimension. Yet, the spatial heterogeneities in the distribution of sediment and sediment transport capacity (largely controlled by water velocity) often result in less sediment being carried by the water than could be ~~theoretically transported (e.g. Lane et al., 2017; Delaney et al., 2018b)~~ transported theoretically (e.g., Lane et al., 2017; Delaney et al., 2018b). As a result, reducing the problem to one dimension omits key processes controlling sediment dynamics because subglacial water flows through spatially distributed networks of cavities and channels across the glacier bed (~~e.g. Werder et al., 2013~~). ~~The one dimensional models to date (e.g., Werder et al., 2013)~~. To date, the one-dimensional models have yielded insights into the creation of eskers (Beaud et al., 2018a; Hewitt and Creyts, 2019), the formation of subglacial canals through which water flows (Walder and Fowler, 1994; Ng, 2000; Kasmalkar et al., 2019), subglacial processes in overdeepenings (Creyts et al., 2013) and the behavior of tidewater glaciers (Brinkerhoff et al., 2017). Yet, describing subglacial sediment transport inherently lends itself to a discretization of bedrock erosion, sediment transport, water flow, and sediment availability in ~~the downstream~~ both the downglacier and transverse dimensions (e.g., x- and y-).

In this manuscript, we present SUGSET\_2D, a ~~new~~-two-dimensional subglacial sediment transport model. The model ~~implements subglacial the~~ includes subglacial sediment transport and bedrock erosion processes. We implement a routing scheme that transports sediment in x- and y- based on the local hydraulic potential gradient. Synthetic cases demonstrate the model's ability to reproduce known processes and yield insight into the spatially-distributed processes responsible for subglacial sediment dynamics. We also apply the model to a real alpine glacier, Griesgletscher in Switzerland. The model was run with hydrology and topography data from the glacier, and measured sediment discharge data ~~are-were~~ used to validate the model. Through these experiments, we explore the importance of two-dimensional sediment connectivity in the subglacial environment.

## 2 Model Description

The model presented here implements a hydraulic model and sediment routing scheme that translates ~~the many of the underpinnings~~ of the one-dimensional subglacial sediment transport model presented in Delaney et al. (2019) to two dimensions. In this section, we ~~review the underpinnings of the model presented in Delaney et al. (2019), describe the~~ describe hydraulic and sediment transport models, explain the implemented water and sediment routing scheme, and outline its numerical implementation in two dimensions.

## 2.1 Hydraulic Model

90 SUGSET\_2D requires a ~~hydraulics~~ hydraulic model as a means to route sediment and water through the subglacial environment. The ~~hydraulics~~ hydraulic model is also needed to evaluate the sediment transport capacity of this water, based upon the hydraulic gradient, channel size, and water flux (~~Table 1, Section 2.2; e.g. Walder and Fowler, 1994; Alley et al., 1997~~) (Table 1, Section 2.2; e.g., Walder and Fowler, 1994; Alley et al., 1997). The hydraulic model is based on the premise that subglacial water flows along the hydraulic potential gradient and ~~that~~ the weight of ice pressurizes water at the bed (Shreve, 95 1972). ~~We simulate~~ This model includes characteristics of an R othlisberger-channel without explicitly describing properties such as creep closure and pressure melt of channel walls.

The hydraulic gradient of a subglacial channel  $\Psi$  (at a certain location and time) can be determined with a known hydraulic diameter  $D_h$  and water discharge  $Q_w$ . The hydraulic gradient can then be determined using the Darcy-Weissbach equation for fluid flow through a pipe

$$\Psi = s f_r \rho_w \frac{Q_w^2}{D_h^5} \quad (1)$$

100 the density of water is  $\rho_w$ , the Darcy-Weissbach friction factor is  $f_r$ , and the channel ~~geometry's~~ cross-sectional geometry, which impacts water pressure, is accounted for by  $s$  (Hooke et al., 1990). ~~We represent~~  $s$  can be represented as as

$$s = \frac{2(\beta - \sin \beta)^2}{\left(\frac{\beta}{2} + \sin \frac{\beta}{2}\right)^4} \quad (2)$$

where  $\beta$  is the central angle of the circular segment representing the channel edge. Smaller values of  $\beta$  result in broad channels and  $\beta = \pi$  results in a semicircular channel. ~~The channel width  $w_c$  is given by~~

$$w_c = 2 \sin \frac{\beta}{2} \sqrt{\frac{2S}{\beta - \sin \beta}},$$

~~where  $S$  is the cross-sectional area of the channel given by~~

$$S = \frac{D_h^2}{2} \frac{\left(\frac{\beta}{2} + \sin \frac{\beta}{2}\right)^2}{\beta - \sin \beta}.$$

To approximate the hydraulic diameter  $D_h$ , we ~~prescribe a melt rate  $\dot{m}_w$  to establish  $Q_w$  and~~ assign a representative water discharge  $Q_w^*$  to  $Q_w$ , by taking a characteristic water discharge over a certain time period prior (hours to days). We assume that the hydraulic diameter of the channel results from this characteristic water discharge we call the source percentile (~~e.f. de Fleurian et al., 2018; Delaney et al., 2019; Nanni et al., 2020~~) ( $s_p$ ; c.f. Gimbert et al., 2016; de Fleurian et al., 2018; Delaney et al., 115 . The response time,  $s_a$  and source percentile ~~remain~~,  $s_p$ , remain consistent throughout the model run. The values for these variables are poorly constrained, yet their impact can be intuited. For instance, short-lived increases in water discharge due to an hour of precipitation will not greatly impact the hydraulic diameter of the subglacial channel, ~~where as~~ whereas prolonged melt would increase the hydraulic diameter.

~~Water storage is not allowed, such that~~  $Q_w^*$  and  $Q_w$  comprise the total instantaneous amount of melt water produced up-glacier, as this hydraulic model does not consider water storage.

~~We then evaluate~~  $D_h$ , the hydraulic diameter given is evaluated from

$$D_h = \left( s f_r \rho_w \frac{Q_w^{*2}}{\Psi^*} \right)^{\frac{1}{5}}. \quad (3)$$

120  $\Psi^*$  is a representative hydraulic gradient at overburden pressure, evaluated using the Shreve potential gradient

$$\Psi^* = \nabla(\rho_i g(z_s - z_b) + \rho_w g z_b), \quad (4)$$

where  $z_s$  and  $z_b$  are surface and bed elevations, respectively,  $\rho_i$  is the density of ice and  $g$  is the gravitational acceleration constant.

With knowledge of  $D_h$ , we insert the instantaneous value of  $Q_w$  into Equation 1 to evaluate the instantaneous hydraulic gradient  $\Psi$ . To prevent unreasonable water pressures when  $Q_w^*$  rapidly increases and  $D_h$  is small, the model limits the minimal cross-sectional area  $S$  to 0.5 hydraulic diameter to 0.3 m<sup>2</sup> (Delaney et al., 2019).

## 2.2 ~~Till-layer~~ Till layer model: bedrock erosion and sediment transport

The model simulates the evolution of a subglacial till layer, which we define as transportable sediment below the glacier due to glacier erosion and fluvial sediment transport. Fluvial sediment transport, in supply- and transport-limited regimes, mobilizes and deposits sediment, adding or removing material from the till layer (Brinkerhoff et al., 2017; Delaney et al., 2019). Conversely, erosive processes such as abrasion and quarrying add material to the layer, while we do not consider processes such as fluvial abrasion that appear to produce minimal sediment (Beaud et al., 2018b). To represent these processes, we implement the Exner Equation (Figure 2; Exner, 1920a,b; Paola and Voller, 2005), a mass conservation relationship, to solve for the till layer height given the erosive and fluvial conditions.

$$\underbrace{\frac{\partial H}{\partial t}}_{\text{till evolution}} = - \underbrace{\nabla \cdot Q_s}_{\text{sediment transport}} + \underbrace{\dot{m}_t}_{\text{bedrock erosion}} \quad (5)$$

$H$  is till thickness and  $t$  is time (Table 1). The first term represents fluvial sediment transport processes, where  $\nabla \cdot Q_s$  represents sediment mobilization in either supply- or transport- limited regimes. The second term captures bedrock erosion processes, where  $\dot{m}_t$  is a bedrock erosion rate.

We evaluate the mobilization of sediment in both supply- and transport- limited conditions. Divergence of the sediment flux is calculated evaluated by approximating  $\nabla \cdot Q_s$  with  $\frac{\nabla \cdot \tilde{Q}_s}{w}$  and using the mobilization scheme from Delaney et al. (2019)

$$\nabla \cdot \tilde{Q}_s = \begin{cases} \frac{Q_{sc} - Q_s}{l} & \text{if } \frac{Q_{sc} - Q_s}{l} \leq \dot{m}_t w \quad \text{(transport-limited)} \quad (6a) \\ 0 & \text{if } H = H_{lim} \quad \& \quad \frac{Q_{sc} - Q_s}{l} \leq 0 \quad (6b) \\ \frac{Q_{sc} - Q_s}{l} \sigma(H) + \dot{m}_t w (1 - \sigma(H)) & \text{otherwise} \quad \text{(supply-limited)} \quad (6c) \end{cases}$$

140  $w$  is the width of a patch of glacier bed ~~perpendicular~~ perpendicular to the direction of water flow over which sediment can be accessed by a channel.  $Q_{sc}$  is sediment transport capacity, or the amount of sediment that could be transported under the given hydraulic conditions.  $l$  is a characteristic length-scale for sediment mobilization, over which sediment mobilization adjusts to sediment transport conditions.  $\sigma$  is a sigmoidal function of  $H$

$$\sigma(H) = \left( 1 + \exp \left( \frac{2 - \Delta\sigma H}{5} \right) \right)^{-1}, \quad (7)$$

145 ~~that which~~ enables smooth transition ~~over the range:  $H = 2\Delta\sigma^{-1} + \Delta\sigma^{-1}$~~  from transport- to supply- limited transport in Equation 6c.  ~~$\Delta\sigma$  is a value below which  $\sigma$  substantially deviates from 1, and reduces sediment mobilization~~ If  $H$  is greater than  $3\Delta\sigma$ , then sediment mobilization is unaffected and the system is in a transport-limited regime. When  $H = \Delta\sigma$ , then  $\sigma(H)$  is close to 0, sediment transport is in a supply-limited regime, and nearly no sediment mobilization takes place.

Condition 6a represents the case where bedrock erosion exceeds sediment mobilization, thus sediment transport exists in a ~~transport-limited~~ transport- limited regime. Condition 6b impedes mobilization or deposition, transporting sediment to the next cell when a till thickness is equal to  $H_{lim}$ , the value of which is chosen to be on the order of maximal change in till height  
150 over the model run ( $\sim 10$  cm). This term prevents unbounded sediment accumulation, as the model does not include physical processes to limit sediment deposition, such as reduced channel size in response to infill of sediment (Perolo et al., 2018). Condition 6c allows sediment mobilization to transition between transport- and supply-limited regimes, limiting sediment mobilization to sediment production term  $\dot{m}_t$  (see below), when  $H$  is small ~~and thus minimal sediment is available for transport~~. With these three conditions, we can evaluate sediment transport in transport- and supply-limited regimes and pass  
155 sediment through the system when till height is large.

We calculate sediment transport capacity  $Q_{sc}$  using the total sediment transport relationship by Engelund and Hansen (1967),

$$Q_{sc} = \frac{0.4}{f_r} \frac{1}{D_m (\frac{\rho_s}{\rho_w} - 1)^2 g^2} \left( \frac{\tau}{\rho_w} \right)^{\frac{5}{2}} w_{c\sim}, \quad (8)$$

where  $\rho_s$  ( $\rho_w$ ) is the bulk density of the sediment (water),  $D_m$  is the mean sediment grain size and  $\tau$  represents the shear stress between the water and the channel bed. ~~We~~

160 The width of the channel floor  $w_c$ , needed to evaluate the surface over which sediment transport may occur, is given by

$$w_c = 2 \sin \frac{\beta}{2} \sqrt{\frac{2S}{\beta - \sin \beta}}, \quad (9)$$

where again  $\beta$  is the Hooke angle controlling channel morphology (Section 2.1),  $S$  is the cross-sectional area of the channel given by

$$S = \frac{D_h^2}{2} \frac{\left( \frac{\beta}{2} + \sin \frac{\beta}{2} \right)^2}{\beta - \sin \beta}. \quad (10)$$

Here, hydraulic diameter  $D_h$  is evaluated from Equation 3.

We also determine the shear stress in Equation 8 through the Darcy-Weisbach formulation:-

$$\tau = \frac{1}{8} f_r \rho_w v^2, \quad (11)$$

165 where  $v = \frac{Q_w}{S}$  is the water velocity. Water discharge  $Q_w$  is calculated by the water flowing above and  $S$  is evaluated in Equation 10. Other sediment transport relationships using shear stress could be exchanged by the model operator (e.g. Meyer-Peter and Müller, (e.g. Meyer-Peter and Müller, 1948)). We chose Engelund and Hansen (1967)'s formulation due to the representation of both suspended and bedload transport.

Source We assume that till armors the bed from erosion (e.g., Alley et al., 2003; Brinkerhoff et al., 2017; Delaney et al., 2019)

170 . In response, the source term  $\dot{m}_t$  is described as,

$$\dot{m}_t = \dot{e} \left(1 - \frac{H}{H_{max}}\right), \quad (12)$$

where  $H_{max}$  is a till height beyond which no further erosion,  $\dot{e}$ , may occur.

We chose to use an empirical relationship with sliding velocity  $u_b$  to describe bedrock erosion,

$$\dot{e} = k_g u_b^{l_{er}}, \quad (13)$$

where  $k_g$  is an erodability constant and  $l_{er}$  is an exponent, which varies from between 0.66 and 3 (Herman et al., 2021).  $u_b$  is assumed to be related to basal shear stress ( $\tau_b$ ; Weertman, 1957) given the following relationship

$$u_b = B_s \tau_b^m, \quad (14)$$

175  $B_s$  is a constant and we assume the exponent  $m$  is equal to 1. We assume that  $\tau_b$  is equal to driving stress (Cuffey and Paterson, 2010)

$$\tau_b = \rho_i g h (\sin \alpha), \quad (15)$$

where  $\rho_i$  is the density of ice,  $h$  is the glacier thickness, and  $\alpha$  is the surface slope of the glacier.

Note that because  $\dot{m}_t$  is a source term, alternative parameterizations of erosion or basal sliding can easily be exchanged for  $\dot{m}_t$ .

## 180 2.3 Spatial and temporal discretization, and parameters

Here, we describe the numerical implementation of the equations presented above, and in particular the routing scheme that enables a two-dimensional representation of subglacial fluvial and till dynamics.

### 2.3.1 Numerical implementation Water and parameters sediment routing and implementation

185 We use a regular grid to discretize the bed assume that sediment and water moves across the glacier bed following the steepest gradient in hydraulic potential. On glaciers, we define the hydraulic potential at a cell  $i$  in the grid,  $\phi_i$ , based upon the elevation

of the glacier bed plus the ice thickness, following Shreve (1972).

$$\phi_i = f_f \rho_i g (z_{s,i} - z_{b,i}) + \rho_w g z_{b,i} , \quad (16)$$

where  $f_f$  is the flotation fraction across the glacier,  $z_s$  is the glacier surface, and  $z_b$  is the glacier bed.

190 With this information, we use a multi-cell routing scheme (Quinn et al., 1991) to establish flow routing based upon the steepest hydraulic potential in Equation 16 and with a single value of  $f_f$  across the glacier bed. We implement this scheme in a similar way as Bovy et al. (2016), but on a regular grid in  $x$  and  $y$  directions, where fluxes can pass to the four surrounding cells sharing an edge. This routing scheme returns a stack ( $s_t$ ; Table 3), which contains information about the order of cells to perform the calculations, along with the number of cells flowing in to a cell (donors;  $n_d$ ), number of cells that a cell contributes (receivers;  $n_r$ ), and the weight of hydraulic potential and water or sediment discharge directed from one cell to another ( $w_d$  or  $w_r$ ).

195 For the first time step, the hydraulic potential  $\phi$  is evaluated under the condition that  $f_f = 1$ . After the first time step, we assume that the flotation fraction, will vary in response to changing hydraulic conditions such as diurnal or seasonal water input (e.g., Iken and Bindschadler, 1986). In turn, to establish an average flotation fraction  $f_f$  across the glacier bed for Equation 16, we use

$$f_f = \text{mean} \left( \frac{\phi_{o,i}}{\rho_i g (z_{s,i} - z_{b,i}) + \rho_w g z_{b,i}} \right) , \quad (17)$$

where the denominator represents the hydraulic potential at overburden pressure ( $f_f = 1$  in Equation 16).

200  $\phi_0$  represents the hydraulic potential evaluated from summing the hydraulic gradient  $\Psi$  in Equation 1 up glacier from its outlet.  $\phi_0$  at each cell  $i$  is evaluated as

$$\phi_{o,i} = \Psi_i \cdot \lambda + \sum_{j=1}^{n_r} (\phi_{0,j} \cdot w_{r,j}) . \quad (18)$$

205 Here,  $\Psi_i$  comes from evaluating Equation 1 from the receiver cell  $j$  of  $i$ ,  $\lambda$  is edge length of a cell on a regular grid,  $n_r$  is the number of receivers that the cell  $i$  has, and  $w_r$  is the proportion of hydraulic potential fed by the upstream cell  $j$ . The operation is executed on a cell by cell basis, beginning at the base of the glacier and moving up the flow paths evaluated in the routing scheme.

Using the routing scheme above, but performing the operation from the top of the glacier, we evaluate the water discharge in a cell  $Q_{w,i}$  from melt upstream as

$$Q_{w,i} = \dot{m}_{w,i} \cdot \delta + \sum_{j=1}^{n_d} Q_{w,j} \cdot w_{d,j} , \quad (19)$$

where  $\dot{m}_w$  is a prescribed meltwater source term in cell  $i$ ,  $n_d$  is the number of cells directing water at cell  $i$ , and  $w_{d,j}$  is the percentage of water flow from cell  $j$  directed at cell  $i$ . **Spatial discretization-**



Sediment mobilization into a cell  $\overline{Q_{s,i}}$  is like-wise computed by implementing Equation 6 from the top of the glacier through the stack as

$$\overline{Q_{s,i}} = \begin{cases} \sum_{j=1}^{n_d} \left( \frac{Q_{sc,j} - Q_{s,j}}{l} \cdot w_{d,j} \right) & \text{if } \sum_{j=1}^{n_d} \left( \frac{Q_{sc,j} - Q_{s,j}}{l} \right) \cdot w_{d,j} \leq \dot{m}_{t,i} \cdot \lambda & (20a) \\ 0 & \text{if } H_j = H_{lim} \ \& \ \frac{Q_{sc,j} - Q_{s,j}}{l} < 0 & (20b) \\ \dot{m}_{t,i} \lambda \left( 1 - \sigma(H) \right) + \sum_{j=1}^{n_d} \left( \frac{Q_{sc,j} - Q_{s,j}}{l} \right) \cdot \sigma(H) w_{d,j} & \text{otherwise} & (20c) \end{cases}$$

210 where  $Q_{sc,j}$  is the sediment transport capacity from cell  $j$  flowing to  $i$ ,  $Q_{s,j}$  is sediment discharge entering from cell  $j$  to cell  $i$ , again  $l$  is a response length scale and  $\lambda$  is cell length.

Sediment discharge  $Q_{s,i}$  out of a cell  $i$  is evaluated as

$$Q_{s,i} = \overline{Q_{s,i}} \cdot \lambda + \sum_{j=1}^{n_d} Q_{s,j} . \quad (21)$$

We evaluate the change in till height at a cell by implementing Equation 5 as

$$\frac{dH_i}{dt} = \frac{-Q_{s,i} + \sum_{j=1}^{n_d} Q_{s,j}}{\delta} + \dot{m}_{t,i} , \quad (22)$$

where again  $\delta$  is cell area.

### 215 2.3.2 Numerics and parameters

Spatial discretization on the regular grid must be substantially smaller than characteristic length-scale,  $l$ , in Equation 6 Equations 6 and 20. We then solve Equation 5 for 22 to establish till height  $H$  for given initial and boundary conditions in response to till production  $\dot{m}_t$  and divergence of the sediment discharge  $Q_s$  using an explicit time integration scheme.

To discretize the problem in time, the model implements the VCABM solver (Hairer et al., 1992; Radhakrishnan and Hind-  
220 marsh, 1993) from the package *DifferentialEquations.jl* (Rackauckas and Nie, 2017) to evolve till layer height  $H$ . This solver implements an adaptive time step and uses a linear multistep method (Adams-Moulton) that is well-suited for to non-stiff problems, which is optimal because of the rapid fluctuations in sediment transport that can occur. We impose a maximum time step of 6 h to ensure that the model captures the response to diurnal variations in melt input. In practice, the solver commonly uses a time step of roughly 20 minutes, which varies depending on sediment transport conditions and solver tolerance. Longer  
225 time steps occur over periods when glacier melt, and thus sediment transport, cease (i.e. , winter months). Table 3 presents the numerical parameters used.

We execute the routing scheme based upon hydraulic conditions to the nearest 6 minutes to improve stability and fill closed basins in hydraulic potential to maintain continuous sediment transport through the domain. Smaller solving tolerances

230 increase the computational time due to 1) increased accuracy of the solution and 2) the reassessment of flow fractions between the adjacent cells, which results in different routing configurations as the model converges.

We impose boundary conditions on the edge cells so no sediment or water enters the domain. At outlet cells, water discharge leaves the domain, as does a flux of sediment leaves the domain, based on sediment transport conditions. Boundary-In other applications, boundary conditions could also be set to represent processes, such as hillslope erosion that route material or glacial lakes, that route sediment or water to the subglacial environment (e.g. Andersen et al., 2015)-(e.g., Andersen et al., 2015). At  
235 the outlet cells, we assume that the hydraulic potential has no ice overburden pressure.

Evolving Equation 5 requires an initial till height,  $H_0$ , chosen by the model user. This initial till height represents material from bedrock erosion created prior to the model initialization. We apply a “~~spin-up~~spin up” procedure to create a reasonable relationship between the amount of fluvial sediment transport and bedrock erosion.

240 New versions of the code are tested against reference cases to ensure consistency. Additionally in each test, we ensure mass conservation by checking that the amount of sediment leaving the system through fluvial transport is consistent with the till height change and erosion occurring under the simulated glacier.

### 2.3.3 Routing algorithm and implementation

~~Sediment and water are routed down the hydraulic gradient using a multi-cell routing scheme (Quinn et al., 1991), implemented in a similar way as Bovy et al. (2016), but instead on a regular grid. Sediment and water moves from one cell to another using a~~  
245 ~~steepest-descent algorithm, based upon the hydraulic potential. This routing scheme returns a stack, which contains information about the order of cells to perform the calculations. The model evaluates the hydraulic potential at every time step, first, the flotation fraction for a cell at a given time is calculated by  $f_f = \frac{\phi_o}{\phi^*}$ , where hydraulic potential  $\phi_o$  comes from~~

$$\phi_o = \phi_o + \sum_{j=1}^{n_r} \Psi_j \cdot \delta^{\frac{1}{2}} \cdot w_{r_j}.$$

250 ~~Here,  $\Psi_j$  comes from Equation 1,  $\delta$  is the area of a cell on a regular grid yielding cell length,  $n_r$  is the number of receivers that the cell has, and  $w_r$  is the proportion of hydraulic potential fed by the upstream cell. The operation is executed on a cell-by-cell basis using the routing scheme above, beginning at the glacier lower elevations and moving up glacier.~~

~~We distribute the mean value of  $f_f$  across the glacier and then implement the routing scheme for the hydraulic potential determined from the Shreve potential as~~

$$\phi = f_f \rho_i g (z_s - z_b) + \rho_w g z_b.$$

255 ~~The node ordering algorithm is executed every time step in response to diurnal variations in water pressure and thus variable routing of subglacial water in response to changing hydraulic conditions (e.g. Iken and Bindshadler, 1986; Chu et al., 2016). However, to improve stability during periods of rapidly changing sediment transport conditions, we reorder the stack, based upon the hydraulic conditions to the nearest 6. Smaller solving tolerances increase the computational time due to 1) increased accuracy of the solution and 2) the reassessment of flow fractions between the adjacent cells, which results in different routing~~

260 configurations as the model converges. We fill closed basins in hydraulic potential to maintain continuous sediment transport through the domain. The model uses an external algorithm, that contains routes flow and fills basins based upon rasterised values of the hydraulic potential.

Using this routing scheme, we are able to evaluate the water discharge in a cell from melt upstream as

$$Q_w = \dot{m}_w \cdot \delta + \sum_{j=1}^{n_r} Q_{w_j} \cdot w_{r_j},$$

265 where  $\dot{m}_w$  is a melt water source term and  $n_r$  is the number of receivers of that cell. The sediment discharge  $Q_s$  into a cell is like-wise computed as

$$Q_s = \sum_{j=1}^{n_r} Q_s \cdot w_{r_j}.$$

$Q_s$  is then used to evaluate the  $\nabla \cdot Q_s$  given Equation 6 and subsequently, the change in till height using Equation 5. In both Equation 19 and ??, the operations are conducted given the node ordering information in the stack, such that the flux in to a cell depends on the flux through the catchment above it.

### 3 Model Application

We use two cases to highlight model viability under increasingly complex situations. First, we apply the model to a synthetic alpine glacier ~~with synthetic hydrology~~ topography with a synthetic hydrologic forcing, based on the Subglacial Hydrology Model Inter-comparison Project (SHMIP; de Fleurian et al., 2018), to illustrate the model's performance in a simplistic scenario. We then apply the model to the topography, and sediment and water discharge at Griesgletscher in the Swiss Alps. We demonstrate the proficiency of the model by comparing sediment transport model output and data (Delaney et al., 2018a). We also identify some drivers of subglacial sediment discharge in the model from these simulations.

#### 3.1 Synthetic alpine cases

##### 3.1.1 Experiment design

280 We run simulations using an alpine glacier geometry ~~and hydrological forcing following~~ , along with the seasonally and diurnally varying hydrological forcing from the SHMIP project experiments (de Fleurian et al., 2018)). The domain is 6000 m on one axis and 1080 m on the other. The resulting geometry approximates the Bench Glacier in Alaska. The U-shaped bed and variable ice thickness mean that variable hydrologic gradients will occur laterally across the glacier and water can be routed across multiple cells.

285 To represent hydrology that varies over seasonally and diurnally, we implement a simple melt-model-spatially distributed melt model, as in SHMIP ( de Fleurian et al., 2018)

$$\dot{m}_w(z_s) = \begin{cases} M_f T(z_s) + \dot{m}_b & \text{if } T(z_s) > 0 \\ \dot{m}_b & \text{if } T(z_s) \leq 0 \end{cases}, \quad (23)$$

where  $M_f = 0.01 \text{ m K}^{-1} \text{ d}^{-1}$  is a melt factor, and  $\dot{m}_b$  is the basal melt rate.  $T(z_s)$  is air temperature  $T$  at elevation  $z_s$ , defined as

$$290 \quad T(z_s) = \left( -A_a \cos\left(\frac{2\pi t}{s_{year}}\right) + A_d \cos\left(\frac{2\pi t}{s_{day}}\right) + \Delta T - 5 \right) \cdot \left( 1 + z_s \frac{dT}{dz} \right), \quad (24)$$

where  $A_a$  and  $A_d$  are the annual and diurnal amplitudes ;-respectively;- in temperature, respectively;  $\Delta T$  is a temperature offset, which is adjusted to control the meltwater inputand;  $s_{day}$  are the number of seconds in one day;  $s_{year}$  is the number of seconds in a yearand;  $\frac{dT}{dz} = -0.0075 \text{ K m}^{-1}$  is the air temperature lapse rate. In this case, we route water directly to the subglacial system at the location where the melt occurs, ignoring-moulins for instance, omitting moulins or crevasses that  
 295 concentrate meltwater delivery to the bed.

We run the model for 12-10 years with a steady climate, then we apply a linear temperature increase for 8 of  $0.5^\circ \text{ a}^{-1}$  for 10 years followed by 10 years of steady temperature at the maximal  $\Delta T$ . We implement the dramatic warming to capture the model's response to variable climatic conditions. The model is initiated with 105 cm of till across the bed. A spin-up over one year of the initial hydrological forcing is applied for 150  
 300 for 5 a or an for computational reasons. In other applications the spin up could be maintained, until the annual change in the till layer height is less than  $10^{-4} \text{ m}$ , well below the annual erosion rate in most glacierized catchments till height was well below commonly accepted glacier erosion rates (Hallet et al., 1996).

### 3.1.2 Model outputs and findings

Simulations show that over seasonal timescales, sediment discharge increases at the onset of melt and decreases shortly there-  
 305 after, prior to the maximum amount of water discharge that occurs in the peak of each melt season (Figure 4). Daily-averaged sediment discharge decreases until the very end of the melt season, when sediment discharge increases very slightly again (Figure 6 b, d, f). This occurs when water stops flowing during the night, allowing sediment to accumulate in the channels from bedrock erosion. Increased sediment discharge at the beginning of the melt season results from greater sediment availability following the growth of the till layer over the winter months, when the small amount of melt limits-prevents substantial  
 310 transport sediment.

Increases in sediment discharge at the onset of melt produced by the model (Figure 4 b, and 6 b, d, f) have been observed for real glaciers (Willis et al., 1996; Swift et al., 2005; Riihimaki et al., 2005; Delaney et al., 2018b) and reproduced in the one-dimensional version of this model (Delaney et al., 2019). However, in SUGSET\_2D, larger diurnal increases in sediment discharge occur near peak daily melt because the area of flowing water expands under the glacier. As a result, increased

315 sediment transport may occur in cells with substantial sediment when hydraulic conditions permit, then abandoned them when  
water is routed to another part of the glacier bed. This allows sediment to be stored in these cells, until the hydraulic conditions  
return and increased sediment transport may return. Such a process is difficult to represent in a one-dimensional model, where  
the many of the cells could be represented together.

Over the course of the simulation, the mean till height ~~decreases and more sediment is expelled from the glacier as the~~  
320 ~~system adjusts to the change in climate~~ continues to decrease throughout the model run (Figure 6). This occurs despite the  
spin-up threshold of  $10^{-4} \text{ m yr}^{-1}$  change in till height per year, highlighting the difficulty in achieving a true equilibrium between  
bedrock erosion and sediment transport ~~a~~ . Exhaustion of sediment is evident in the middle of the glacier where much of the  
water flows resulting from the spin up procedure (Figure 4,e). Till height decrease accelerates following the onset of increased  
melt at year 12. With the new steady climate reached at year 20, the annual quantities of sediment discharge began to decrease.  
325 This occurs as the system approaches a stable relationship between sediment transport and bedrock erosion.

Interestingly, the model recreates "first-flush" events of increased sediment discharge early in the melt season (Figure 6),  
followed by decreased sediment discharge (Swift et al., 2005; Delaney et al., 2018b). This seasonal evolution in sediment  
discharge is attributed to increased access to subglacial sediment early in the season, followed by decreased access as flow  
becomes increasingly channelized (e.g. Willis et al., 1996; Swift et al., 2005). As melt begins in the spring, sediment discharge  
330 ~~increases largely due to increased sediment transport high on the glacier~~ 6 e f. However, the decreasing till height through  
the model run results from mobilization on the margins of the glacier, where water flow in a warmer climate occurs more  
often. Increased water flow on the upper reaches of the glacier results in increased sediment transport (Figure 4). ~~However,~~  
~~maximum values of sediment discharge during "first-flush" events decrease because sediment transport also occurs over that~~  
~~time. By the end of the simulation, winter transport is large enough to prevent the till layer from growing. This maintains a~~  
335 ~~sediment reservoir available for transit when melt increases. Note that the model does not couple ice dynamics to sub-glacial~~  
~~hydrology, so erosive potential, water discharge and the subglacial area will decrease as well in response to the changing~~  
~~climate. Additionally, increased subglacial water discharge could enhance sliding, and thus erosion, may occur following the~~  
~~onset of melt in the spring (Ugelvig et al., 2018).~~ b and a greater area of the bed where sediment transport occurs (Figure 6 e, f).

340 For the cases described above, bedrock erosion relies only on driving stress and till thickness. Sliding and bedrock erosion  
did not vary seasonally with increased subglacial water discharge (Figure 6 a, b, Section 3.1). This causes sediment to accu-  
mulate during the winter months, which subsequently provides ample material for transport when melt increases in the spring.  
~~The model's bedrock erosion scheme is most applicable to land-terminating glaciers and over long time scales when driving~~  
~~stress likely exerts a primary control on glacier sliding (e.g. Weertman, 1957; ?). However, by coupling subglacial hydrology~~  
345 ~~to erosion Ugelvig et al. (2018) shows that erosion varies seasonally and abrasion largely occurs solely during the summer~~  
~~months. Additionally, in the case presented above, sediment production occurs primarily near the glacier front, where driving~~  
~~stress, and thus sliding, is highest (Figure 3, a).~~

To test the effects of spatially variable erosion and the role of hydrology, we present two additional cases to supplement  
the alpine glacier case above, *ORIGINAL*. ~~The first~~ One additional case, *SEASON*, simulates bedrock erosion by ~~increasing~~

350 ~~sliding only allowing sliding, and thus erosion,~~ during the summer months ~~(e.g. Iken and Bindshadler, 1986), (e.g., Iken and Bindshadler,~~  
; the same erosion relationship is applied as the case ~~as in~~ Section 3.1. In this case, however, erosion only occurs when the  
amount of water input substantially exceeds the background basal melt input rate, that is present in the winter. ~~In the second~~  
~~We choose this case to capture the seasonal variations in bedrock erosion (Ugelvig et al., 2018). In the other additional~~ case,  
355 ~~CONST~~, bedrock erosion remains constant over the entirety of the glacier at a rate of ~~±2~~ mm a<sup>-1</sup>, ~~independent of glacier sliding~~  
~~velocity.~~

The *ORIGINAL* case discharges over ~~1162011.620~~ m<sup>3</sup> of sediment per year, while the *SEASON* case ~~discharged~~ discharges  
only 60% of that value due to the absence of bedrock erosion during the winter months. The *CONST* case discharged 7320 m<sup>3</sup>  
of sediment over the year. *CONST*'s quantity of sediment discharge results in ~~roughly 1 a~~ catchment-scaled height change  
~~roughly 1.1~~ mm a<sup>-1</sup> ~~erosion rate~~ due to decreased erosion efficiency with till height (Equation 12 ~~and the limited portion of the~~  
360 ~~bed over which sediment transport occurs-~~), ~~instead of prescribed bedrock erosion rate of 2~~ mm a<sup>-1</sup>. Additionally, the spatial  
~~disparity of where sediment is produced at the glacier bed compared to the location of sediment transport further reduces the~~  
~~catchment scaled height change~~ (Figure 6 e, f).

Over the three cases, sediment discharge increases at the onset of melt and substantially decreases by the end of the melt sea-  
son due to sediment exhaustion. In *ORIGINAL* (Figure 6 a, b), more sediment discharge occurs compared to the alternate cases  
365 (*SEASON* and *CONST*). The increased sediment discharge in *ORIGINAL* is ~~due-1~~ due to the prolonged period over which  
bedrock erosion occurs adding more sediment to the layer and 2) ~~that because~~ bedrock erosion occurs low on the glacier where  
much sediment transport takes place (Figure 6 d), compared to the *CONST* case. The peak sediment discharge in *CONST* (Fig-  
ure 6 e, f) occurs slightly earlier in the season, due to the increased amounts of sediment on the ~~lower glacier margins~~ glacier's  
~~lower portions.~~

## 370 3.2 Griesgletscher

### 3.2.1 Experiment design

We also simulate Griesgletscher in the Swiss Alps using topographic data from ~~(Delaney et al., 2019)~~ Delaney et al. (2019).  
Hourly water discharge from the glacier was modeled in Delaney et al. (2018a). Here, we use the discharge time series from  
2009–2017. Subglacial sediment discharge from the glacier was determined for four different time periods since fall 2011 by  
375 differencing bathymetry maps ~~and considering proglacial erosion quantities~~ (Delaney et al., 2018a). To estimate surface melt  
across the glacier with respect to elevation, we use,

$$\dot{m}_w(x, y) = \dot{b}^0 + \gamma(z_s(x, y) - z_s^0). \quad (25)$$

~~Here,~~  $\gamma$  is the mass balance gradient and  $z_s^0$  represents the glacier's lowest elevation.  $\dot{b}^0$  represents the melt rate at the glacier's  
lowest extent.  $\dot{b}^0$  was evaluated numerically at each water discharge value using the hypsometry of the glacier.

380 We apply a parameter search over a range of values of sediment grain size ( $D_m$ ; ~~representing~~ a primary control on fluvial  
transport of subglacial sediment), sliding rate factor ( $B$ ; ~~representing~~ a control on bedrock erosion), and the initial till height

condition ( $H_0$ ; ~~to approximate, representing~~ the effects of existing quantities of sediment below the glacier). 100 simulations were run with randomly selected parameters ~~from, each with~~ a uniform distribution. No ~~spin-up spin up~~ was applied in this case, because of the wide range of  $H_0$  values explored.

385 The wall time for a single model run averaged 8.9 h, and each run for a parameter set was executed on a single CPU. Instead of applying the mean flotation fraction across the glacier, as was done in the previous cases, the maximum value was applied with an upper limit of 1.

We only considered model outputs resulting in a perfect rank correlation across the four data collection periods and an error less than ~~80,000~~ 131,000  $\text{m}^{-3}$ . For the case presented below, we show the simulation with the lowest absolute error between  
390 model output and the sediment transport data.

### 3.2.2 Model outputs and findings

The ~~model parameter search yields an optimum grain size parameter  $D_m$  of 2 cm, sliding parameter  $B$  of  $2.05 \times 10^{-11}$  MPa  $\text{m s}^{-1}$  and initial till height  $H_0$  of 2.5 mm. The model's ability to reproduce the validation data largely depends on the grain size parameter,  $D_m$ . Compared to  $D_m$ , the sliding parameters and initial condition parameters ( $B$  and  $H_0$ ) have a reduced  
395 influence in representing the data, given that similar values of  $B$  and  $H_0$  can produce largely different results in the context of  $D_m$  (Figure 7 a, b, c).~~

~~The optimized parameter combination, along with others, reproduces the interannual variability in sediment discharge from the Griesgletscher (Figure 7 g). The absolute error between the model optimum model run and the measurements is roughly 62,600  $\text{m}^3$ . The model represents the last three measured yearly sums of sediment discharge well, but it has trouble reconciling  
400 the elevated sediment discharge in 2012 and 2013 (Figure 7). This suggests that processes not adequately represented in the model are responsible for the increase in sediment transport, such as activation of new patches of the glacier bed or the relocation of channels (e.g. Zechmann et al., 2020), potentially due to changes to glacier surface topography that cause alternative flow paths below the glacier. Furthermore, glacier sliding, remains constant over the model run, in turn, the results do not explicitly account for seasonal or interannual variability in bedrock erosion (e.g. Herman et al., 2015).~~

~~The error from this parameter search is slightly less than half of the 131,300  $\text{m}^3$  total sediment discharged from the Griesgletscher over this time period (Delaney et al., 2018a), and the error is slightly more than the 58,300  $\text{m}^3$  from the best model run of the one-dimensional model in Delaney et al. (2019). The model runs captures the third period from late 2014 to late 2015 well. However, in contrast to the ensemble model runs in Delaney et al. (2019), this model's ability to reproduce the validation data largely depends on the grain size parameter,  $D_m$ . Compared to Delaney et al. (2019), the sliding parameters  
410 and initial condition parameters ( $B$  and  $H_0$ ) have a minimal influence here when tuned to the data the runs systematically overestimate the second and fourth periods and generally underestimate the high discharge period from late 2011 until late 2013 (Figure 7. The dependence on grain size for SUGSET\_2D results from the subglacial sediment connectivity parameterized in this two-dimensional version of the model. The channelized nature of flow means that sediment transport may only occur over a relatively narrow patch of the glacier bed g).~~

415 The best performing model run shows strong temporal variability in sediment discharge. Peaks in sediment discharge occur during the short-lived increases in water discharge (Figure 9). As sediment grain size decreases, sediment from locations of 8 a). Despite the strong dependence on grain size and fluvial transport of sediment in the parameter search, sediment transport capacity  $Q_{sc}$  still remains roughly an order of magnitude higher than sediment discharge  $Q_s$  (Figure 8 a, b). The steep section of the glacier experiences sediment depletion over the model run, as do several patches of the glacier bed with relatively small  
420 water velocity and discharge can more easily be transported to the main glacier channel and be expelled from the glacier. In a one-dimensional model, sediment access occurs over the entire width of the glacier bed. Thus, the bedrock erosion or sediment production term (largely controlled by sliding rate factor  $B$ ) represents this process, and increased sediment production results in greater connectivity.

The size and shape of the subglacial channels contribute to the discharge of sediment glacier bed near the over-deepening and high on the glacier (Figure 9 c d). On some parts of the upper glacier, as well. The sediment transport due to the velocity of subglacial water is limited by the channel width in smaller channels ( $w_c$ , Equation 8). For this reason, sediment exhaustion occurs mainly in main channels, where channel widths are sufficiently large to allow substantial sediment transport (Figure 3). Conversely, sediment persists in patches of the glacier bed where water velocity could be high, but insufficient channel size effectively reduces sediment transport capacity. Increasing the friction factor  $f_t$  increases the area of the glacier bed over which  
430 water with substantial velocity flows in SUGSET\_2D. Thus the model has trouble capturing interannual variability because sediment exhaustion does not occur over a substantial portion of the glacier bed bedrock erosion grows the till layer beyond the initial condition in the absence of substantial sediment transport.

The value of  $B$ , from the parameter search, results in a average an average sliding velocity of  $39 \text{ m a}^{-1}$  of glacier sliding across the glacier bed, and the range of values for  $B$  in the parameter search result in mean sliding velocities roughly between  
435  $14 \text{ ma}^{-1}$  and  $70 \text{ ma}^{-1}$ . Yet, due to the low dependence of sediment transport from the glacier on  $B$ , other values could perform well but are not captured in the relatively small number of model runs herein. However, because sediment (Equation 14). Because sediment production decreases with till height (Equation 12), sediment production is limited to the narrow patches of the glacier bed where minimal till persists and bedrock erosion may occur. As a result, the model requires more sliding to produce the equivalent amount of sediment with more till at the bed, even though the sliding and erosion parameters applied  
440 here are within a well constrained range. At the same time, the limited spatial extent of glacier erosion and sediment transport points to a need to evaluate the precise location of bedrock erosion and the impact of subglacial till layers on bedrock erosion in future research.

The best performing model run shows strong temporal variability in sediment discharge (Figure 8), with water discharges from the glacier above roughly  $2^{-3-1}$  responsible for much of the sediment transport. Despite the strong dependence on grain size and fluvial transport of sediment in the inversion, sediment transport capacity  $Q_{sc}$  remains roughly an order of magnitude higher than sediment discharge ( $Q_{sc}$ ). The steep section of the glacier experiences sediment depletion over the model run, as do several channels near the over-deepening and high on the glacier (Figure 9 c d). On some parts of the upper glacier, bedrock erosion in the absence of substantial sediment transport is visible. With changing melt patterns or evolving glacier hydraulic gradients, this sediment could be mobilized and increase sediment discharge down glacier.



## 450 4 Model limitations

The lack of knowledge regarding the spatial distribution of subglacial sediment makes selecting an initial value of  $H$  difficult. The slow rate of basal erosion means that an equilibrium between fluvial sediment transport and bedrock erosion will likely take centuries to attain, if such an equilibrium may even exist in light of variable climatic, and thus glacier, conditions. Should an equilibrium ~~exist~~be present (e.g., Herman et al., 2018; Delaney and Adhikari, 2020), it is probably outside of a feasible computational time ~~given of this model given its~~ current processing speeds(e.g. Herman et al., 2018; Delaney and Adhikari, 2020)

In addition to selecting an initial value of  $H$ , we also limit the thickness at which the till must stop accumulating (Equation 6b,  $H_{lim}$ ) due to changes in the hydraulic potential caused by channel infill of sediment. We assume that this value is on the order of tens of centimeters (Table 2), based upon available observations (Perolo et al., 2018). While the impact of a ~~till-layer~~till layer on bedrock abrasion remains uncertain, we expect that sediment of a certain thickness will armor the bed, preventing erosion (Alley et al., 2003). In turn, we limit erosion with till thickness to a threshold (5 cm), ~~on-of~~ the same order ~~of-as~~  $H_{lim}$  to improve computational time. Additionally, the model does not consider the interactions between fluvial ~~transport-of sediment~~sediment transport and debris concentrations in subglacial ice, which may be important for sub-glacial sediment transport (e.g. Ugelvig et al., 2018)(e.g., Ugelvig et al., 2018).

465 SUGSET\_2D also contains 20 parameters (Table 2 and 3). ~~These parameters have only~~ In the available literature, these parameters have been partially constrained using inverse methods (Brinkerhoff et al., 2016) as well as detailed modeling and measurements (e.g. Chen et al., 2018; Covington et al., 2020; Pohle et al., 2022)(e.g., Chen et al., 2018; Covington et al., 2020; Pohle et al.

The routing method we use assumes that water ~~solely flows~~ flow direction is in response to the ~~hydraulic~~ Shreve potential (Section 2.3.1). ~~Our parameterization does include the impact of a channel's size on the hydraulic potential. It also does~~ Therefore, it does not explicitly simulate the evolution of efficient and inefficient subglacial drainage systems over the course of the season, or the inheritance of existing subglacial canals or channels (Figure 3; e.g. Werder et al., 2013; Zechmann et al., 2020) (Figure 3; e.g., Werder et al., 2013; Zechmann et al., 2020). Furthermore, a response time of the subglacial channel is chosen prior to simulations to improve computational time, compared to a more sophisticated~~representation or,~~ but computationally ~~more expensive,~~ representation of processes in an R-channel (e.g. Röthlisberger, 1972)model (e.g., Röthlisberger, 1972).

## 5 Implications

Results of both the one-dimensional model (SUGSET; Delaney et al., 2019) and SUGSET\_2D highlight the importance of simulating the spatial heterogeneities in bedrock erosion, sediment availability, and sediment transport capacity. Yet, in ~~SUGSET, only~~ the one-dimensional version of SUGSET, sediment can be accessed from the till layer (e.g. Equation 6e) and ~~variations in sediment access along the glacier flow line impact sediment transport across the entire glacier width, perpendicular to the glacier flow line.~~ In SUGSET\_2D, sediment access and transport ~~is-are~~ not averaged over the glacier width. Rather, by

considering the spatial distribution in water discharge and sediment availability laterally below a glacier, the model evaluates where heterogeneities may persist and their impact on subglacial sediment dynamics (Figures 6 and 9).

485 ~~Large diurnal and seasonal fluctuations in sediment transport in the synthetic alpine glacier case result from diurnal and seasonal variations in water routing and thus increased sediment availability because sediment transport only occurs over a patch of bed for a short amount of time (Section 3.1)~~ In SUGSET\_2D, large diurnal increases in sediment discharge occur near peak daily melt because the area of flowing water expands under the glacier (Figure 6 b, d, f). As a result, increased sediment transport can occur in regions of the glacier bed with substantial sediment when hydraulic conditions permit, then the patch of bed is abandoned when water is routed to another part of the glacier bed (Video supplement). This allows sediment to  
490 be stored in these regions until the hydraulic conditions return and increased sediment transport. Such a process is difficult to represent in a one-dimensional model, where the entire width of the glacier is represented together (Figures 4 b and 6 b, d, f; Video supplement). For instance here, diurnal fluctuations in sediment discharge in the middle of the season can be 50% above the mean value ~~;~~ (Figure 6 b, d, f), which aligns more closely with some field observation of sediment discharge ~~(e.g., Swift et al., 2005; Delaney et al., 2018b) compared to~~ (e.g., Swift et al., 2005; Delaney et al., 2018b) compared to  
495 the one-dimensional version of SUGSET (c.f. Delaney et al., 2019). Furthermore, the results show that the location of bedrock erosion, processes in the ~~till layer~~ till layer, and the timing of melt all play an important role in the quantity of sediment discharge and the peak sediment discharge that is reached.

In the final case, we compared model runs across a parameter space to sediment discharge data from Griesgletscher in the Swiss Alps (Section 3.2). ~~These results depended solely~~ The limited ability of the model to capture the large sediment discharge  
500 from the first time period and the minimum sediment discharge in the second and fourth time periods show that processes not adequately represented in the model are responsible for the increase in sediment transport at this time (Figure 7). Such processes may include activation of new patches of the glacier bed or the relocation of channels (e.g., Zechmann et al., 2020), potentially due to changes to glacier surface topography that cause alternative flow paths below the glacier. Furthermore, glacier sliding remains constant over the model run. In turn, the results do not explicitly account for seasonal or interannual variability in  
505 bedrock erosion (e.g., Herman et al., 2015).

Model performance at Griesgletscher depends greatly on sediment grain size ~~compared to~~ compared to other parameters such as the initial till condition or bedrock erosion (Figure 7). Grain size is a strong control in the SUGSET\_2D because it modulates how easily sediment ~~patches only is mobilized in patches of the bed only occasionally~~ accessed by sub-glacial flow during the melt season ~~are mobilized~~. This process cannot be fully considered in a one-dimensional model, though ~~it is important~~  
510 even in this processes seems important on this relatively small and shallow alpine glacier. These results show that connectivity between subglacial channels and distal sediment patches is a strong control on sediment discharge from the subglacial system. This is especially so because main flow paths can be evacuated of sediment (Figure 9 c, d). Thus these flow paths contribute to the catchment's sediment discharge only through the production of sediment through erosion (Equation 12). The connectivity between the main channels and distal sources of sediment could be through the transport of small sediments as applied here,  
515 but may also occur through other processes not considered in the model, such as till deformation ~~(e.g., Damsgaard et al., 2020)~~ (e.g., Damsgaard et al., 2020).

Lastly, the model demonstrates the complex nature of subglacial sediment transport and the transitions between supply- and transport- limited regimes. Sediment discharge depends not only on hydrology but also on the sediment availability. Equivalent values of water input and sediment transport capacity below the glacier result in simulated sediment discharge that vary over orders of magnitude (Figure 10, a). In turn, using solely the water discharge or sediment transport capacity (e.g., Equation 8) fails to consider the changes to sediment availability caused by sediment transport, especially when changes to sediment storage can take place over seasons to decades. Finding ways to evaluate these difficult to measure parameters could be key to improving our understanding of subglacial sediment transport.

## 6 Conclusions

~~This manuscript presents~~ We present a two-dimensional subglacial sediment transport model, SUGSET\_2D, that evolves a ~~till layer~~ till layer in response to subglacial hydrology. Model cases utilize geometries and hydrological forcings from a synthetic and a real alpine glacier. The model captures sediment transport in supply- and transport- limited regimes. Results from both cases point to the need to quantify the spatial distribution of subglacial sediment and water when simulating sediment discharge expelled from glaciers. Model outputs reproduce many observed subglacial sediment processes.

Despite the model's ability to reproduce observations, it relies on a large number of poorly constrained parameters. ~~To~~ For instance, to our knowledge, only one study has quantified till thickness at a single point below a glacier (Truffer et al., 2000). These observations are limited due to the difficulty of making direct observations at glacier beds. The initial till height,  $H_0$ , in the model, therefore, must be chosen ~~carefully~~ carefully-thoughtfully because the system ~~can remember this initial condition for centuries. The interaction of bedrock erosion and fluvial sediment transport also leads hysteresis in the system~~ remains impacted by this condition throughout the model run.

~~Two-dimensional sediment transport models can represent more~~ This two-dimensional sediment transport model can represent several observed characteristics of subglacial sediment discharge compared to ~~the~~ the one-dimensional ~~models~~ version. SUGSET\_2D routes water and sediment using the Shreve potential and a spatially uniform flotation-fraction that evolves in time in the real glacier case (e.g., Section 3.2). Future work may consider using a coupled model of channelized and distributed drainage networks (Hewitt, 2013; Werder et al., 2013). Increasing the sophistication of the subglacial hydrology model may better evaluate the locations of high ~~potential sediment transport~~ sediment transport capacity. Such models could even be run offline if the operator assumes, as we do, that rates of change in till height are small compared to the evolution in cross-section of the subglacial conduit.

Our simulations highlight that increased glacier melt does not necessarily result in commensurate changes to sediment discharge unless new previously inaccessible subglacial sediment patches are accessed by meltwater. Additionally, results demonstrate the role of spatially varying water routing and lateral sediment connectivity in subglacial sediment discharge. Further efforts should constrain the role of ~~climate change on glacial dynamics~~, changing glacial dynamics on erosion and sediment transport. Further modeling and observational studies are needed to better constrain the timescales over-which these processes occur in ~~response to climate change~~ a changing climate.

550 *Code availability.* The code library and illustrative examples are available at <https://bitbucket.org/IanDelaney/sugset.jl/src/id-2d>. The running and plotting scripts used in the cases herein are stored at [https://bitbucket.org/IanDelaney/2d\\_runners/src/master/](https://bitbucket.org/IanDelaney/2d_runners/src/master/).

*Video supplement.* Videos of a prior model version's application to Griesgletcher are available at <https://bit.ly/3nPvVUI>, demonstrating model behavior. Similar videos of the current model version will be transferred to a permanent location pending acceptance.

*Author contributions.* ID designed the study, developed the model, ran the cases and lead writing the manuscript. LA assisted with the writing the manuscript and provided key advice designing and troubleshooting the model. FH provided guidance with implementing and designing the model and preparing the manuscript.

*Competing interests.* The authors declare no competing interests.

*Acknowledgements.* We thank J. Braun, B. Bovy, F. De Doncker, [G. Jouvet](#), S. N. Lane, G. ~~Jouvet~~, G. Prasicek and M. Werder for fruitful discussions and insightful comments. We are also grateful to Grégoire Mariéthoz and the Scientific Computing and Research Support Unit at 560 Université de Lausanne for providing computing resources. I. [Delaney was funded in part by SNF Project No. PZ00P2\\_202024. I.](#) Overeem, S. Hergarten and ~~an anonymous reviewer~~ [two anonymous reviewers](#) provided thoughtful and constructive comments that greatly improved this manuscript.

## References

- Alley, R. B., Cuffey, K. M., Evenson, E. B., Strasser, J. C., Lawson, D. E., and Larson, G. J.: How glaciers entrain and transport basal sediment: physical constraints, *Quaternary Science Reviews*, 16, 1017–1038, [https://doi.org/10.1016/S0277-3791\(97\)00034-6](https://doi.org/10.1016/S0277-3791(97)00034-6), 1997.
- Alley, R. B., Lawson, D. E., Larson, G. J., Evenson, E. B., and Baker, G. S.: Stabilizing feedbacks in glacier-bed erosion, *Nature*, 424, 758–760, <https://doi.org/10.1038/nature01839>, 2003.
- Andersen, J. L., Egholm, D. L., Knudsen, M. F., Jansen, J. D., and Nielsen, S. B.: The periglacial engine of mountain erosion– Part 1: Rates of frost cracking and frost creep, *Earth Surface Dynamics*, 3, 447–462, <https://doi.org/10.5194/esurf-3-447-2015>, <https://esurf.copernicus.org/articles/3/447/2015/>, 2015.
- Beaud, F., Flowers, G., and Venditti, J. G.: Modeling sediment transport in ice-walled subglacial channels and its implications for esker formation and pro-glacial sediment yields, *Journal of Geophysical Research: Earth Surface*, 123, 1–56, <https://doi.org/10.1029/2018JF004779>, 2018a.
- Beaud, F., Venditti, J., Flowers, G., and Koppes, M.: Excavation of subglacial bedrock channels by seasonal meltwater flow, *Earth Surface Processes and Landforms*, 43, 1960–1972, <https://doi.org/10.1002/esp.4367>, 2018b.
- Bhatia, M. P., Kujawinski, E. B., Das, S. B., Breier, C. F., Henderson, P. B., and Charette, M. A.: Greenland meltwater as a significant and potentially bioavailable source of iron to the ocean, *Nature Geoscience*, 6, 274, 2013.
- Bovy, B., Braun, J., and Demoulin, A.: A new numerical framework for simulating the control of weather and climate on the evolution of soil-mantled hillslopes, *Geomorphology*, 263, 99 – 112, <https://doi.org/https://doi.org/10.1016/j.geomorph.2016.03.016>, 2016.
- Brinkerhoff, D., Truffer, M., and Aschwanden, A.: Sediment transport drives tidewater glacier periodicity, *Nature Communications*, 8, 90, <https://doi.org/10.1038/s41467-017-00095-5>, 2017.
- Brinkerhoff, D. J., Meyer, C. R., Bueler, E., Truffer, M., and Bartholomaus, T. C.: Inversion of a glacier hydrology model, *Annals of Glaciology*, 57, 84–95, 2016.
- Chen, Y., Liu, X., Gulley, J. D., and Mankoff, K. D.: Subglacial Conduit Roughness: Insights From Computational Fluid Dynamics Models, *Geophysical Research Letters*, 45, 11,206–11,218, <https://doi.org/10.1029/2018GL079590>, 2018.
- Chu, W., Creyts, T. T., and Bell, R. E.: Rerouting of subglacial water flow between neighboring glaciers in West Greenland, *Journal of Geophysical Research: Earth Surface*, 121, 925–938, <https://doi.org/10.1002/2015JF003705>, 2016.
- Church, M. and Ryder, J. M.: Paraglacial sedimentation: a consideration of fluvial processes conditioned by glaciation, *Geological Society of America Bulletin*, 83, 3059–3072, 1972.
- Cook, S., Swift, D., Kirkbride, M., Knight, P., and Waller, R.: The empirical basis for modelling glacial erosion rates, *Nature communications*, 11, 1–7, <https://doi.org/10.1038/s41467-020-14583-8>, 2020.
- Covington, M. D., Gulley, J. D., Trunz, C., Mejia, J., and Gadd, W.: Moulin Volumes Regulate Subglacial Water Pressure on the Greenland Ice Sheet, *Geophysical Research Letters*, 47, e2020GL088 901, <https://doi.org/https://doi.org/10.1029/2020GL088901>, <https://agupubs.onlinelibrary.wiley.com/doi/abs/10.1029/2020GL088901>, 2020.
- Creyts, T. T., Clarke, G. K. C., and Church, M.: Evolution of subglacial overdeepenings in response to sediment redistribution and glaciohydraulic supercooling, *Journal of Geophysical Research: Earth Surface*, 118, 423–446, 2013.
- Cuffey, K. M. and Paterson, W. S. B.: *The Physics of Glaciers*, Butterworth-Heinemann, Burlington, MA, USA, Forth edn., 2010.
- Damsgaard, A., Goren, L., and Suckale, J.: Water pressure fluctuations control variability in sediment flux and slip dynamics beneath glaciers and ice streams, *Communications Earth & Environment*, 1, 1–8, <https://doi.org/10.1038/s43247-020-00074-7>, 2020.

- 600 de Fleurian, B., Werder, M. A., Beyer, S., Brinkerhoff, D., Delaney, I., Dow, C., Downs, J., Hoffman, M., Hooke, R., Seguinot, J., and Sommers, A.: SHMIP The Subglacial Hydrology Model Intercomparison Project, *Journal of Glaciology*, 64, 897–916, <https://doi.org/10.1017/jog.2018.78>, 2018.
- Delaney, I. and Adhikari, S.: Increased subglacial sediment discharge during century scale glacier retreat: consideration of ice dynamics, glacial erosion and fluvial sediment transport, *Geophysical Research Letters*, p. e2019GL085672, <https://doi.org/10.1029/2019GL085672>,  
605 2020.
- Delaney, I., Bauder, A., Huss, M., and Weidmann, Y.: Proglacial erosion rates and processes in a glacierized catchment in the Swiss Alps, *Earth Surface Processes and Landforms*, 43, 765–778, <https://doi.org/10.1002/esp.4239>, 2018a.
- Delaney, I., Bauder, A., Werder, M. A., and Farinotti, D.: Regional and annual variability in subglacial sediment transport by water for two glaciers in the Swiss Alps, *Frontiers in Earth Science*, <https://doi.org/10.3389/feart.2018.00175>, 2018b.
- 610 Delaney, I., Werder, M., and Farinotti, D.: A Numerical Model for Fluvial Transport of Subglacial Sediment, *Journal of Geophysical Research: Earth Surface*, 124, 2197–2223, <https://doi.org/10.1029/2019JF005004>, 2019.
- Egholm, D., Nielsen, S., Pedersen, V., and Lesemann, J.-E.: Glacial effects limiting mountain height, *Nature*, 460, 884–887, <https://doi.org/10.1038/nature08263>, 2009.
- Egholm, D. L., Pedersen, V. K., Knudsen, M. F., and Larsen, N. K.: Coupling the flow of ice, water, and sediment in a glacial landscape  
615 evolution model, *Geomorphology*, 141, 47–66, 2012.
- Engelund, F. and Hansen, E.: A monograph on sediment transport in alluvial streams, Tech. rep., Technical University of Denmark, Copenhagen, Denmark, 1967.
- Exner, F. M.: Über die Wechselwirkung zwischen Wasser und Geschiebe in flüssen, *Abhandlungen der Akademie der Wissenschaften, Wien*, 134, 165–204, 1920a.
- 620 Exner, F. M.: Zur Physik der Dünen, *Abhandlungen der Akademie der Wissenschaften, Wien*, 129, 929–952, 1920b.
- Felix, D., Albayrak, I., Abgottspon, A., and Boes, R. M.: Suspended sediment measurements and calculation of the particle load at HPP Fieschertal, *IOP Conference Series: Earth and Environmental Science*, 49, 122 007, <https://doi.org/10.1088/1755-1315/49/12/122007>, <http://stacks.iop.org/1755-1315/49/i=12/a=122007>, 2016.
- Gimbert, F., Tsai, V. C., Amundson, J. M., Bartholomaeus, T. C., and Walter, J. I.: Subseasonal changes observed in subglacial channel  
625 pressure, size, and sediment transport, *Geophysical Research Letters*, 43, 3786–3794, 2016.
- Hairer, E., Nørsett, S. P., and Wanner, G.: Solving ordinary differential equations I: nonstiff problems, vol. 1, Springer Science & Business, <http://link.springer.com/book/10.1007/978-3-540-78862-1>, 1992.
- Hallet, B.: A theoretical model of glacial abrasion, *Journal of Glaciology*, 23, 39–50, 1979.
- Hallet, B., Hunter, L., and Bogen, J.: Rates of erosion and sediment evacuation by glaciers: A review of field data and their implications,  
630 *Global and Planetary Change*, 12, 213–235, [https://doi.org/10.1016/0921-8181\(95\)00021-6](https://doi.org/10.1016/0921-8181(95)00021-6), 1996.
- Harbor, J., Hallet, B., and Raymond, C.: A numerical model of landform development by glacial erosion, *Nature*, 333, 347, 1988.
- Hawkings, J., Wadham, J., Tranter, M., Raiswell, R., Benning, L., Statham, P., Tedstone, A., Nienow, P., Lee, K., and Telling, J.: Ice sheets as a significant source of highly reactive nanoparticulate iron to the oceans, *Nature communications*, 5, 1–8, <https://doi.org/10.1038/ncomms4929>, 2014.
- 635 Herman, F., Beaud, F., Champagnac, J., Lemieux, J. M., and Sternai, P.: Glacial hydrology and erosion patterns: a mechanism for carving glacial valleys, *Earth and Planetary Science Letters*, 310, 498–508, <https://doi.org/10.1016/j.epsl.2011.08.022>, 2011.

- Herman, F., Beysac, O., Brughelli, M., Lane, S. N., Leprince, S., Adatte, T., Lin, J. Y. Y., Avouac, J. P., and Cox, S. C.: Erosion by an alpine glacier, *Science*, 350, 193–195, <https://doi.org/10.1126/science.aab2386>, 2015.
- 640 Herman, F., Braun, J., Deal, E., and Prasicsek, G.: The Response Time of Glacial Erosion, *Journal of Geophysical Research: Earth Surface*, 123, 801–817, <https://doi.org/10.1002/2017JF004586>, <https://agupubs.onlinelibrary.wiley.com/doi/abs/10.1002/2017JF004586>, 2018.
- Herman, F., De Doncker, F., Delaney, I., Prasicsek, G., and Koppes, M.: The impact of glaciers on mountain erosion, *Nature Reviews Earth & Environment*, 2, 422–435, <https://doi.org/10.1038/s43017-021-00165-9>, 2021.
- Hewitt, I. and Creyts, T.: A model for the formation of eskers, *Geophysical Research Letters*, 46, 6673–6680, <https://doi.org/10.1029/2019GL082304>, 2019.
- 645 Hewitt, I. J.: Seasonal changes in ice sheet motion due to melt water lubrication, *Earth Planetary Science Letters*, 371–372, 16 – 25, <https://doi.org/10.1016/j.epsl.2013.04.022>, 2013.
- Hooke, R. L., Laumann, T., and Kohler, J.: Subglacial Water Pressures and the Shape of Subglacial Conduits, *Journal of Glaciology*, 36, 67–71, <https://doi.org/10.3189/S0022143000005566>, 1990.
- Humphrey, N. and Raymond, C.: Hydrology, erosion and sediment production in a surging glacier: Variegated Glacier, Alaska, 1982–83, *Journal of Glaciology*, 40, 539–552, 1994.
- 650 Iken, A. and Bindschadler, R. A.: Combined measurements of subglacial water pressure and surface velocity of Findelengletscher, Switzerland: conclusions about drainage system and sliding mechanism, *Journal of Glaciology*, 32, 101–119, 1986.
- Iverson, N. R.: Laboratory simulations of glacial abrasion: comparison with theory, *Journal of Glaciology*, 36, 304–314, <https://doi.org/10.3189/002214390793701264>, 1990.
- 655 Iverson, N. R.: A theory of glacial quarrying for landscape evolution models, *Geology*, 40, 679–682, <https://doi.org/10.1130/G33079.1>, 2012.
- Kasmalkar, I., Mantelli, E., and Suckale, J.: Spatial heterogeneity in subglacial drainage driven by till erosion, *Proceedings of the Royal Society A: Mathematical, Physical and Engineering Sciences*, 475, 20190259, <https://doi.org/10.1098/rspa.2019.0259>, 2019.
- Koppes, M., Hallet, B., Rignot, E., Mouginot, J., Wellner, J. S., and Boldt, K.: Observed latitudinal variations in erosion as a function of glacier dynamics, *Nature*, 526, 100–103, 2015.
- 660 Lane, S. N., Bakker, M., Gabbud, C., Micheletti, N., and Saugy, J.: Sediment export, transient landscape response and catchment-scale connectivity following rapid climate warming and alpine glacier recession, *Geomorphology*, 277, 210 – 227, <https://doi.org/10.1016/j.geomorph.2016.02.015>, 2017.
- Li, D., Lu, X., Overeem, I., Walling, D. E., Syvitski, J., Kettner, A. J., Bookhagen, B., Zhou, Y., and Zhang, T.: Exceptional increases in fluvial sediment fluxes in a warmer and wetter High Mountain Asia, *Science*, 374, 599–603, <https://doi.org/10.1126/science.abi9649>, 665 2021.
- Li, D., Lu, X., Walling, D., Zhang, T., Steiner, J., Wasson, R., Harrison, S., Nepal, S., Nie, Y., Immerzeel, W., et al.: High Mountain Asia hydropower systems threatened by climate-driven landscape instability, *Nature Geoscience*, 15, 520–530, 2022.
- Mao, L., Dell’Agnese, A., Huincahe, C., Penna, D., Engel, M., Niedrist, G., and Comiti, F.: Bedload hysteresis in a glacier-fed mountain river, *Earth Surface Processes and Landforms*, 39, 964–976, <https://doi.org/10.1002/esp.3563>, 2014.
- 670 Meyer-Peter, E. and Müller, R.: Formulas for bedload transport, in: *Hydraulic Engineering Reports*, International Association for Hydro-Environment Engineering and Research, 1948.
- Milner, A., Khamis, K., Battin, T., Brittain, J., Barr and, N., Füreder, L., Cauvy-Fraunié, S., Gíslason, G., Jacobsen, D., Hannah, D., et al.: Glacier shrinkage driving global changes in downstream systems, *Proceedings of the National Academy of Sciences*, 114, 9770–9778, 2017.

- 675 Nanni, U., Gimbert, F., Vincent, C., Gräff, D., Walter, F., Piard, L., and Moreau, L.: Quantification of seasonal and diurnal dynamics of subglacial channels using seismic observations on an Alpine glacier, *The Cryosphere*, 14, 1475–1496, <https://doi.org/10.5194/tc-14-1475-2020>, 2020.
- Ng, F. S. L.: Canals under sediment-based ice sheets, *Annals of Glaciology*, 30, 146–152, 2000.
- Paola, C. and Voller, V. R.: A generalized Exner equation for sediment mass balance, *Journal of Geophysical Research: Earth Surface*, 110,   
680 <https://doi.org/10.1029/2004JF000274>, <https://agupubs.onlinelibrary.wiley.com/doi/abs/10.1029/2004JF000274>, 2005.
- Perolo, P., Bakker, M., Gabbud, C., Moradi, G., Rennie, C., and Lane, S. N.: Subglacial sediment production and snout marginal ice uplift during the late ablation season of a temperate valley glacier, *Earth Surface Processes and Landforms*, 0, 1–68, <https://doi.org/10.1002/esp.4562>, 2018.
- Pohle, A., Werder, M. A., Gräff, D., and Farinotti, D.: Characterising englacial R-channels using artificial moulins, *Journal of Glaciology*, p.   
685 1–12, <https://doi.org/10.1017/jog.2022.4>, 2022.
- Prasicek, G., Herman, F., Robl, J., and Braun, J.: Glacial Steady State Topography Controlled by the Coupled Influence of Tectonics and Climate, *Journal of Geophysical Research: Earth Surface*, 123, 1344–1362, <https://doi.org/https://doi.org/10.1029/2017JF004559>, 2018.
- Prasicek, G., Hergarten, S., Deal, E., Herman, F., and Robl, J.: A glacial buzzsaw effect generated by efficient erosion of temperate glaciers in a steady state model, *Earth and Planetary Science Letters*, 543, 116 350, <https://doi.org/10.1016/j.epsl.2020.116350>, 2020.
- 690 Quinn, P., Beven, K., Chevallier, P., and Planchon, O.: The prediction of hillslope flow paths for distributed hydrological modelling using digital terrain models, *Hydrological processes*, 5, 59–79, 1991.
- Rackauckas, C. and Nie, Q.: *DifferentialEquations.jl*—A Performant and Feature-Rich Ecosystem for Solving Differential Equations in Julia, *Journal of Open Research Software*, 5, 15, <https://doi.org/10.5334/jors.151>, 2017.
- Radhakrishnan, K. and Hindmarsh, A. C.: Description and use of LSODE, the Livermore solver for ordinary differential equations, Reference   
695 Publication 1327, NASA, 1993.
- Riihimäki, C. A., MacGregor, K. R., Anderson, R. ., Anderson, S. P., and Loso, M. G.: Sediment evacuation and glacial erosion rates at a small alpine glacier, *Journal of Geophysical Research: Earth Surface (2003–2012)*, 110, <https://doi.org/10.1029/2004JF000189>, 2005.
- Röthlisberger, H.: Water pressure in intra- and subglacial channels, *Journal of Glaciology*, 11, 177–203, 1972.
- Seguinot, J. and Delaney, I.: Last-glacial-cycle glacier erosion potential in the Alps, *Earth Surface Dynamics*, 9, 923–935,   
700 <https://doi.org/10.5194/esurf-9-923-2021>, 2021.
- Shields, A.: *Anwendung der Aehnlichkeitsmechanik und der Turbulenzforschung auf die Geschiebebewegung*, PhD Thesis Technical University Berlin, 1936.
- Shreve, R. L.: Movement of water in glaciers, *Journal of Glaciology*, 11, 205–214, 1972.
- Swift, D. A., Nienow, P. W., and Hoey, T. B.: Basal sediment evacuation by subglacial meltwater: suspended sediment transport from Haut   
705 Glacier d’Arolla, Switzerland, *Earth Surface Processes and Landforms*, 30, 867–883, <https://doi.org/10.1002/esp.1197>, 2005.
- Thapa, B., Shrestha, R., Dhakal, P., and Thapa, B. S.: Problems of Nepalese hydropower projects due to suspended sediments, *Aquatic Ecosystem Health & Management*, 8, 251–257, <https://doi.org/10.1080/14634980500218241>, 2005.
- Truffer, M., Harrison, W. D., and Echelmeyer, K. A.: Glacier motion dominated by processes deep in underlying till, *Journal of Glaciology*, 46, 213–221, 2000.
- 710 Ugelvig, S. V., Egholm, D. L., Anderson, R. S., and Iverson, N. R.: Glacial Erosion Driven by Variations in Meltwater Drainage, *Journal of Geophysical Research: Earth Surface*, 123, <https://doi.org/10.1029/2018JF004680>, 2018.



- Wadham, J., Hawking, J., Tarasov, L., Gregoire, L., Spencer, R., Gutjahr, M., Ridgwell, A., and Kohfeld, K.: Ice sheets matter for the global carbon cycle, *Nature communications*, 10, 1–17, <https://doi.org/10.1038/s41467-019-11394-4>, 2019.
- 715 Walder, J. S. and Fowler, A.: Channelized subglacial drainage over a deformable bed, *Journal of Glaciology*, 40, 3–15, <https://doi.org/10.3189/S0022143000003750>, 1994.
- Weertman, J.: On the sliding of glaciers, *Journal of Glaciology*, 3, 33–38, 1957.
- Werder, M. A., Hewitt, I. J., Schoof, C. G., and Flowers, G. E.: Modeling channelized and distributed subglacial drainage in two dimensions, *Journal of Geophysical Research: Earth Surface*, 118, 2140–2158, <https://doi.org/10.1002/jgrf.20146>, 2013.
- 720 Willis, I. C., Richards, K. S., and Sharp, M. J.: Links between proglacial stream suspended sediment dynamics, glacier hydrology and glacier motion at Midtdalsbreen, Norway, *Hydrological Processes*, 10, 629–648, 1996.
- Zechmann, J., Truffer, M., Motyka, R., Amundson, J., and Larsen, C.: Sediment redistribution beneath the terminus of an advancing glacier, Taku Glacier (T'aakú Kwáan Sí't'i), Alaska, *Journal of Glaciology*, p. 1–15, <https://doi.org/10.1017/jog.2020.101>, 2020.

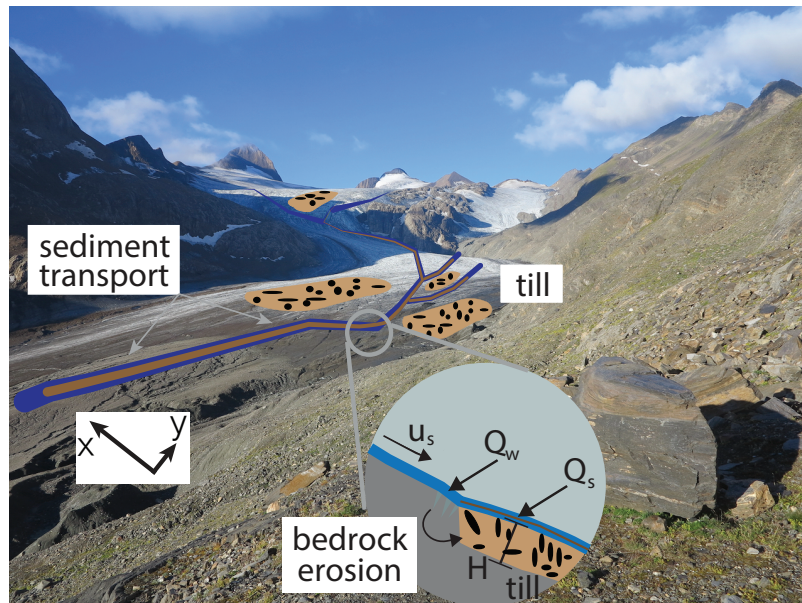


**Figure 1.** Cartoon of erosional and sediment transport processes considered in model [below-overlaid on](#) image of Griesgletscher in 2016. Bedrock erosion scales with sliding speed ( $u_s$ ) and adds material to the till layer with thickness  $H$ , while water ( $Q_w$ ) transports sediment ( $Q_s$ ) fluvially, if sediment persists in that location of the glacier bed and fluvial transport conditions are sufficient.

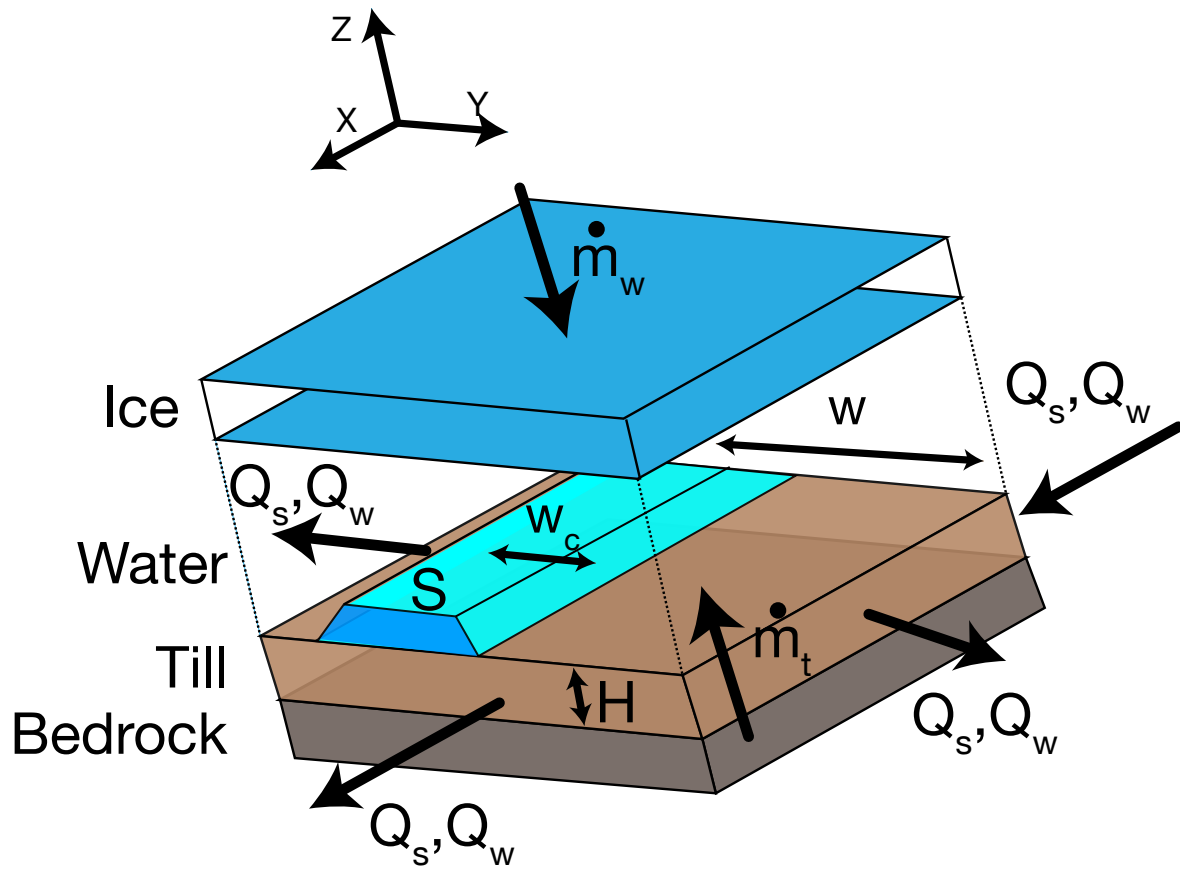


**Figure 2.** Illustration of terms in Equation 5, detailing the layers of bedrock, till, water and ice. Characteristics of the subglacial channel are also noted, but shown in one ~~dimension~~dimension for clarity.

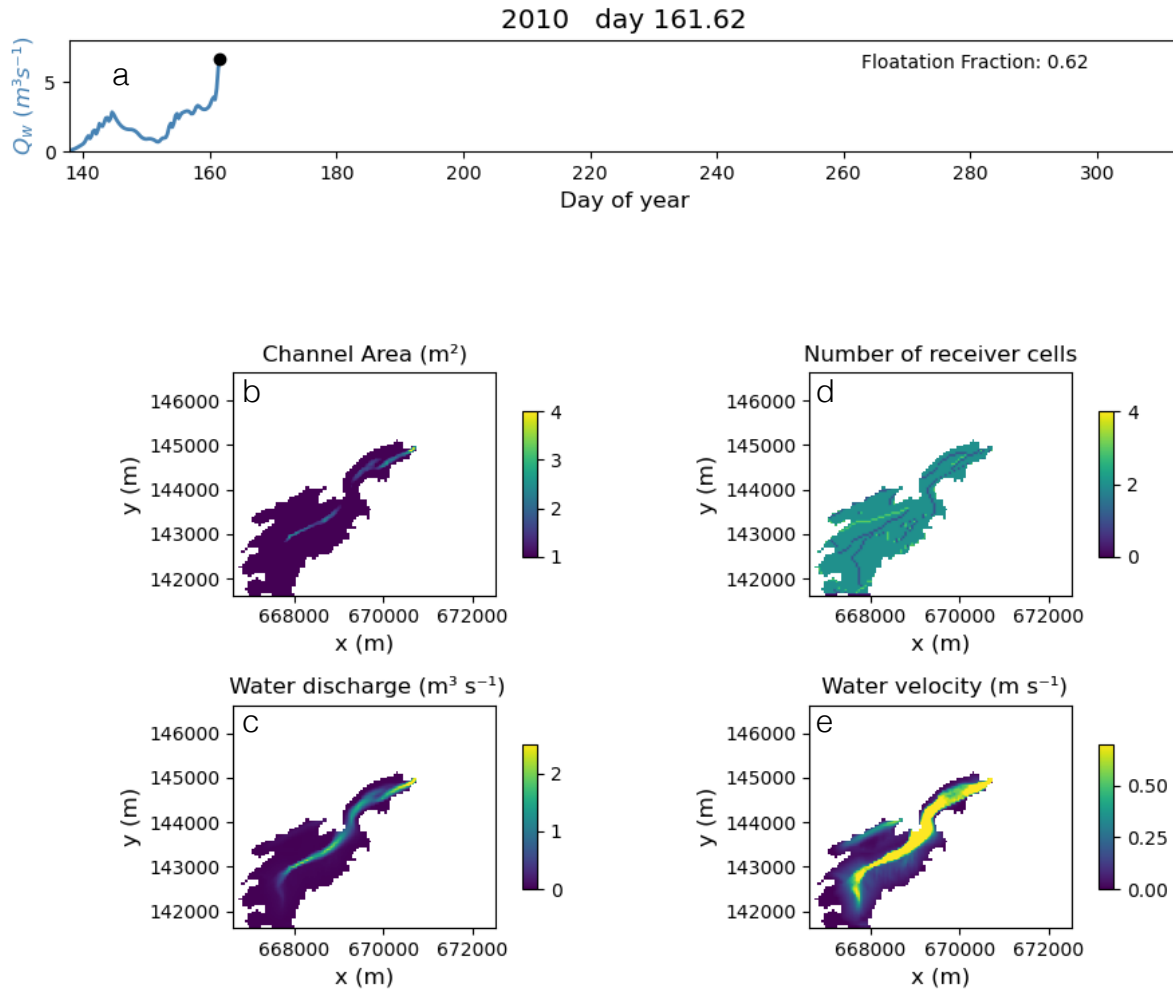


**Figure 3.** Example of model parameters and variables for the ~~snap-shot~~ ~~snap\_shot~~ of the Griesgletscher ~~test-case~~ ~~case~~ Section 3.2. Water discharge from the catchment and glacier floatation fraction (a). Channel cross-sectional area  $S$  (b) with distributed water discharge (c), the number of receivers cells,  $r_t$  for a given cell (d), and the water velocity (e). Conditions ~~b-d~~ ~~b-e~~ evolve with different hydrological conditions (e.g. a) over the glacier run. ~~High-water-velocities-persist-at-this-time-step-due-to-rapid-increase-in-water-discharge-(a)-~~

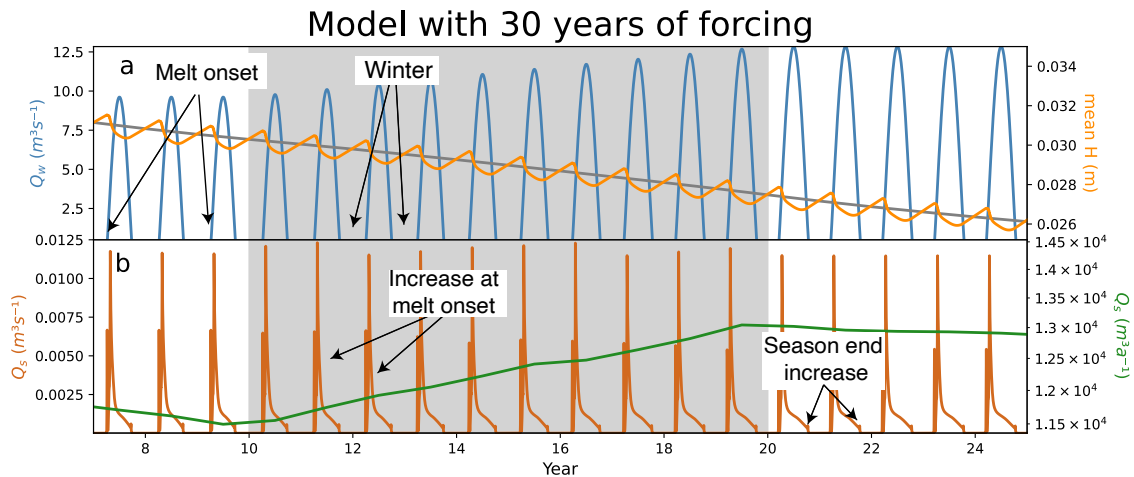
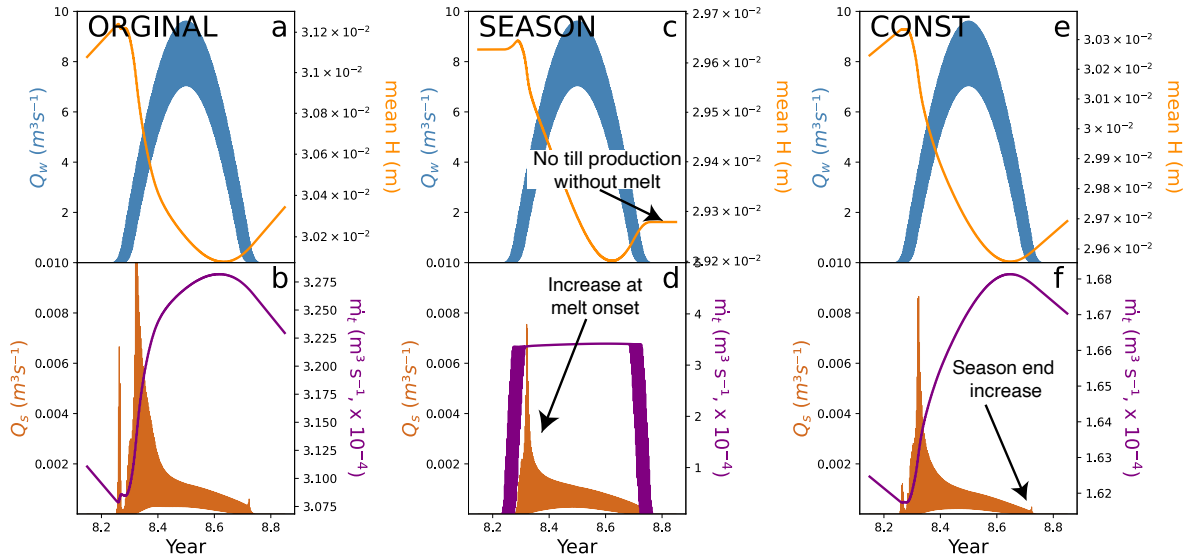


**Figure 4.** Model output from alpine topography and forcing over a 30 year run with diurnal and seasonal variations in melt input. Grey box represents time period of increasing glacier melt. a) Seasonally varying water discharge ( $Q_w$ ) increases from year 10 to 20, while till height ( $H$ ) decreases. b) Sediment Annual sediment discharge (green) increases over this time period with increasing melt, with highest sediment discharge occurring in years 14–17 year 19, when increasing glacier melt can access new sediment sources high on the glacier's greatest. Following Once the increase in temperature new climate stabilizes, melt persists year-around, so annual sediment accumulated during the winter months is no longer available, and thus the glacier does not experience periods of high sediment discharge, although annual sums might be stabilizes at a higher level than before.



Annual response to different erosion-till production patterns across the glacier, ~~although diminishing bedrock erosion with respect to till height is still in place given Equation 12.~~ (a,b) Conventional model setup, where sediment is produced ~~year-around~~ year-round ORIGINAL. This results in the peak amounts of sediment discharge occur in scenario 1 (a,b) where large amounts of sediment accumulated at the glacier terminus during the winter months. (c,d) Equivalent setup to previous, except sediment is only produced in summer months, when water is present at the glacier bed SEASON. ~~Thus, Note that~~ till height remains constant over the winter months. (e,f) Steady erosion of  $1 \text{ mm a}^{-1}$  across the entire glacier, with no spatial or temporal variability in sediment production CONST. ~~Yet~~

Annual response to different erosion-till production patterns across the glacier, ~~although diminishing bedrock erosion with respect to till height is still in place given Equation 12.~~ (a,b) Conventional model setup, where sediment is produced ~~year-around~~ year-round ORIGINAL. This results in the peak amounts of sediment discharge occur in scenario 1 (a,b) where large amounts of sediment accumulated at the glacier terminus during the winter months. (c,d) Equivalent setup to previous, except sediment is only produced in summer months, when water is present at the glacier bed SEASON. ~~Thus, Note that~~ till height remains constant over the winter months. (e,f) Steady erosion of  $1 \text{ mm a}^{-1}$  across the entire glacier, with no spatial or temporal variability in sediment production CONST. ~~Yet~~

**Figure 5.** Spatial view of subglacial sediment transport (a), water discharge (c), till layer height prior to increased melt (b) and after increased melt (d). Spatial discontinuities in the distribution of water and sediment discharge in plots (a) and (c) result from the depletion of subglacial till beneath the glacier. Following the increase in melt, sediment transport increased so that it exceeded bedrock erosion. We have included an animation of this figure in the video supplement.

Annual response to different erosion-till production patterns across the glacier, ~~although diminishing bedrock erosion with respect to till height is still in place given Equation 12.~~ (a,b) Conventional model setup, where sediment is produced ~~year-around~~ year-round ORIGINAL. This results in the peak amounts of sediment discharge occur in scenario 1 (a,b) where large amounts of sediment accumulated at the glacier terminus during the winter months. (c,d) Equivalent setup to previous, except sediment is only produced in summer months, when water is present at the glacier bed SEASON. ~~Thus, Note that~~ till height remains constant over the winter months. (e,f) Steady erosion of  $1 \text{ mm a}^{-1}$  across the entire glacier, with no spatial or temporal variability in sediment production CONST. ~~Yet~~

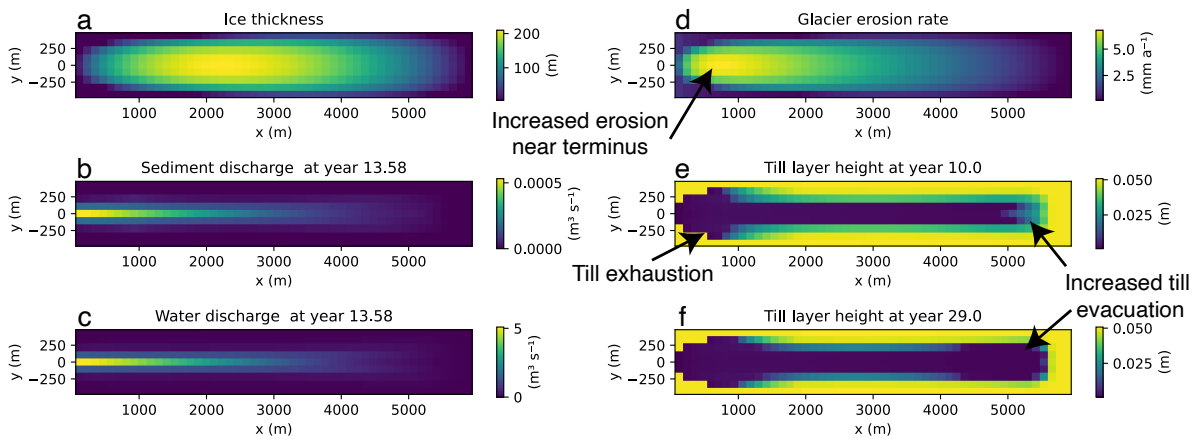


**Figure 6.** Spatial view of subglacial sediment transport (a), the different bedrock erosion scenarios each demonstrate water discharge (c), till layer height prior to increased melt (b) and after increased melt (d). Spatial differences in the distribution of water and sediment discharge at in plots a) and c) result from the onset-depletion of melt and subsequent exhaustion over subglacial till beneath the course glacier. We have included an animation of this figure in the seasonvideo supplement.

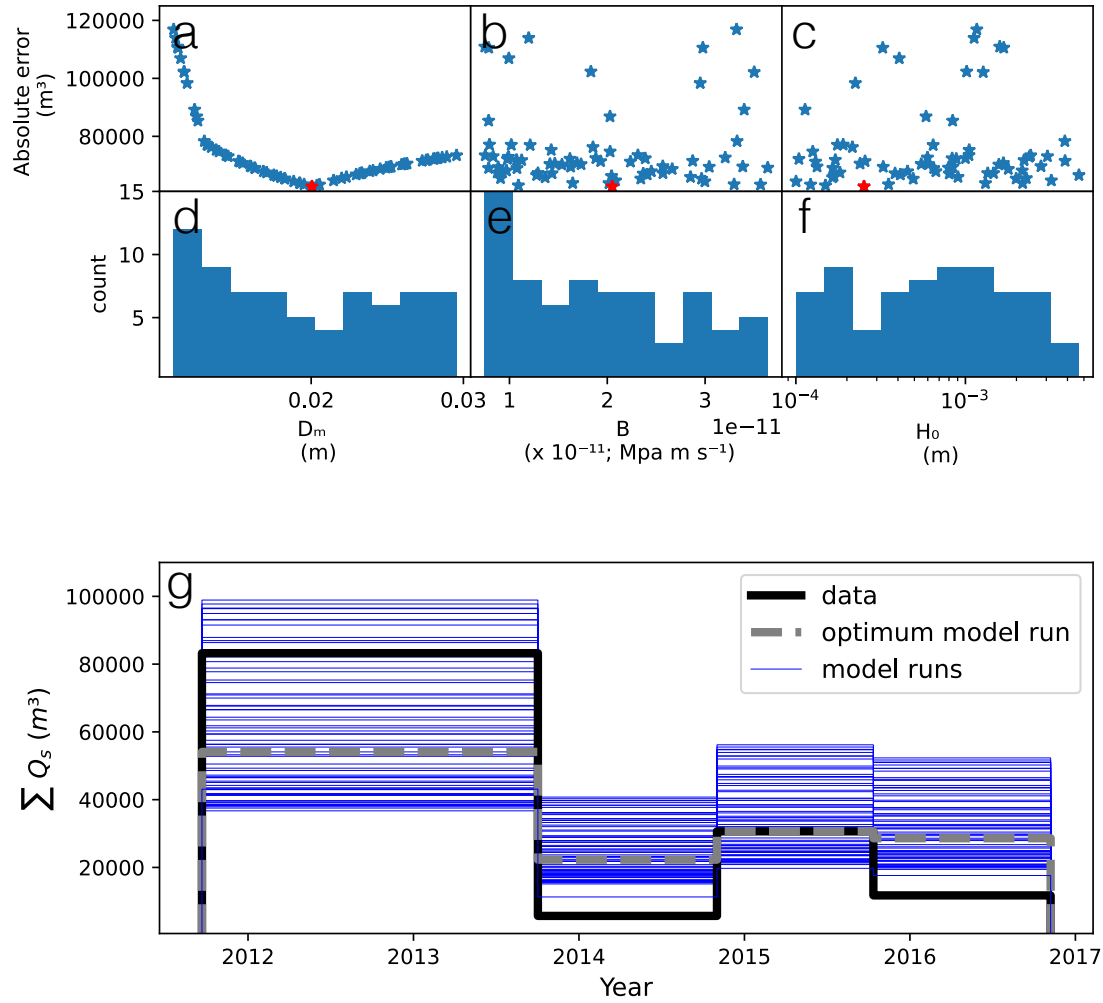


**Figure 7.** Results of the parameter search (column-1a, b, c), the frequency of parameter values that produced a rank correlation of 1 (column-2d, e, f) and the best fit model run amongst the parameter combinations (column-3g). The Red stars represent optimum parameter combination. Blue lines represent all model fails to adequately capture outputs, while gray line represents the 2012–2013 period probably due to processes not considered in the framework optimum parameter combination.



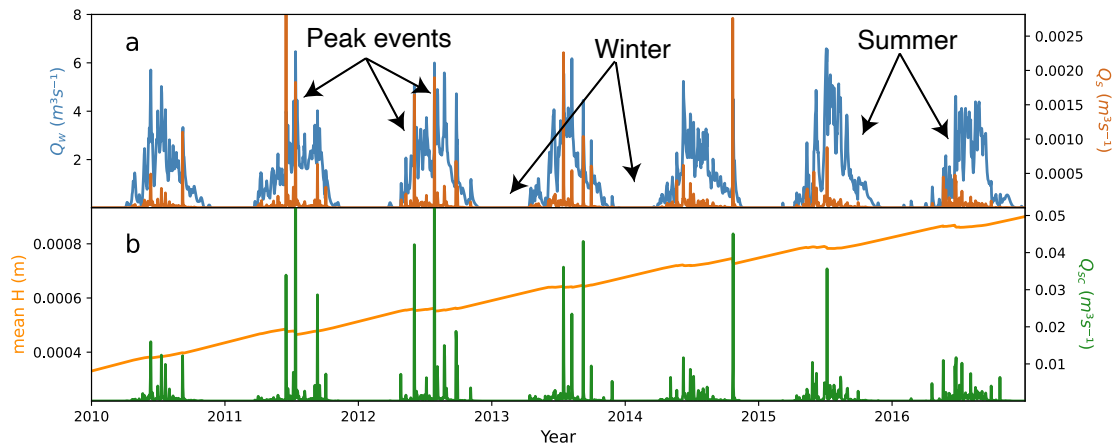


**Figure 8.** Water discharge, an input modeled for Griesgletscher in (Delaney et al., 2018b), and sediment discharge, output of the model, from Griesgletscher (a). ~~Below is modeled outputs of sediment~~ Sediment transport capacity and average till height (b) is below. Note that sediment discharge capacity is roughly one order of magnitude larger than sediment transport discharge. Additionally, the ~~reduction~~ increase in till height  $H$  through this model run shows that sediment is ~~transported from the glacier bed~~ produced at a greater rate than it is ~~produced~~ transported from the glacier bed.

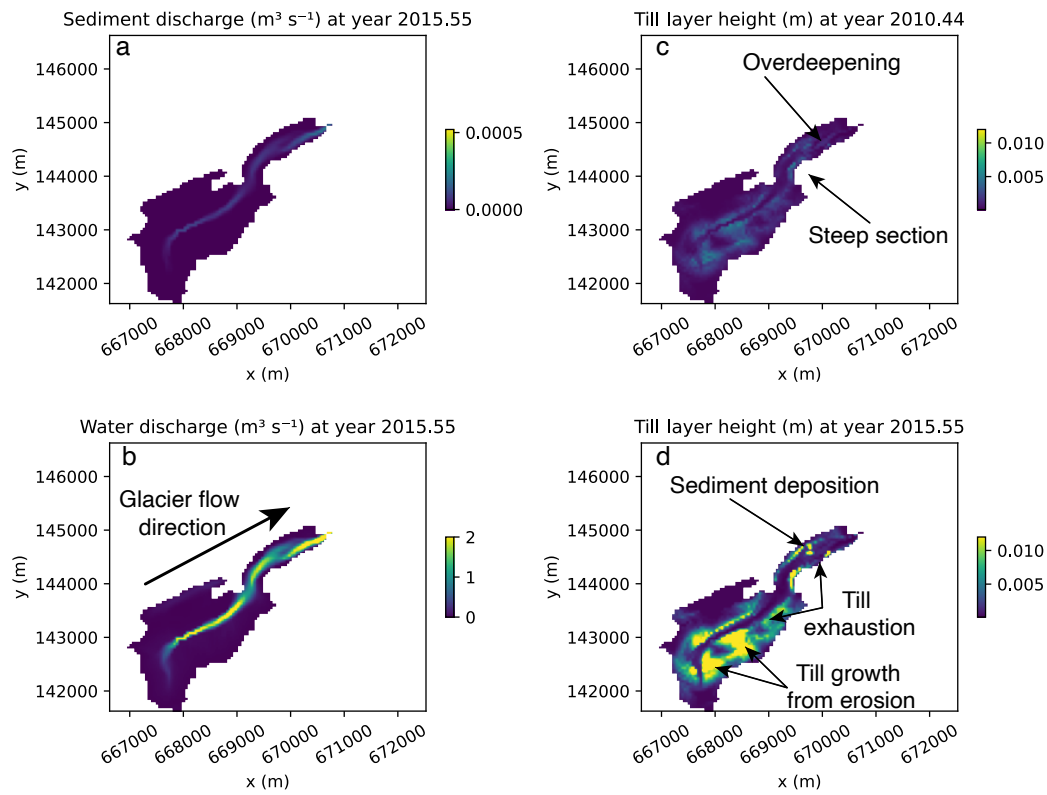


**Figure 9.** Spatial view of characteristics from the ~~select~~-Griesgletscher model run. Figure 1 shows images of this glacier. Subglacial sediment transport (a) and water discharge (c) are highly variable across the bed. Till layer height ~~change~~ changes substantially from the beginning of the model run (c) to after the model run (d). We ~~point out~~ identify the ~~over-deepening~~ overdeepening near the glacier terminus as well as as a steep section connected the upper and lower glacier. Over this time, till exhaustion in regions of high water flow ~~are~~ is visible, while regions of sediment deposition and till growth from glacier erosion can be identified. We have included an animation of this figure in the video supplement.

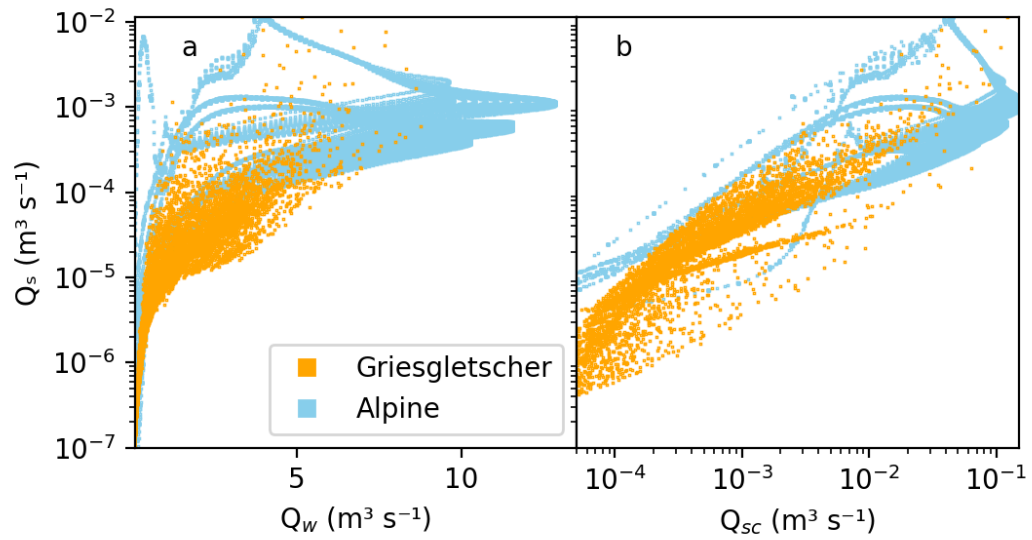


**Figure 10.** Model outputs of sediment discharge from the glacier compared to water discharge (a) and sediment transport capacity (b).

**Table 1.** Model variables

Name	Symbol	Units
Horizontal (x,y) , vertical and time coordinates	$x, y, z, t$	m, m, m, s
Surface and bed elevation	$z_s, z_b$	m, m, m
Glacier surface slope	$\alpha$	-
Channel hydraulic diameter	$D_h$	m
Width of channel floor	$w_c$	m
Channel cross-sectional area	$S$	m <sup>2</sup>
Water discharge (instantaneous)	$Q_w$	m <sup>3</sup> s <sup>-1</sup>
Water source term	$\dot{m}_w$	m s <sup>-1</sup>
Representative water discharge	$Q_w^*$	m <sup>3</sup> s <sup>-1</sup>
Hydraulic potential	$\phi$	Pa
Gradient of $\phi$	$\Psi$	Pa m <sup>-1</sup>
Representative gradient of $\phi$	$\Psi^*$	Pa m <sup>-1</sup>
Flotation fraction	$f_f$	-
Water velocity	$v$	m s <sup>-1</sup>
Water shear-stress	$\tau$	Pa
Till source term	$\dot{m}_t$	m s <sup>-1</sup>
Sediment discharge	$Q_s$	m <sup>3</sup> s <sup>-1</sup>
Sediment discharge capacity	$Q_{sc}$	m <sup>3</sup> s <sup>-1</sup>
Glacier sliding velocity	$u_b$	m s <sup>-1</sup>
<u>Basal shear stress</u>	$\mathcal{T}_b$	MPa
Erosion rate	$\dot{e}$	m s <sup>-1</sup>
Till layer height	$H$	m
Mass-balance rate at terminus	$\dot{b}^0$	m s <sup>-1</sup>

**Table 2.** Physical model parameters and constants

Name	Symbol	Value	Units
Darcy-Weisbach friction factor	$f_r$	Alpine: 15; Gries: 5	-
Hooke angle of channel	$\beta$	<del>22.5</del> 30	°
Source percentile	$s_p$	Alpine: 0.75; Gries: .2	-
Source average time	<del><math>s_a</math></del>	<del>2.5</del> Alpine: 1.5 Alpine: 2.5; Gries: 0.54.5	d
Sediment-uptake $e$ -folding length	$l$	100	m
Sediment grain mean diameter	<del><math>D_{m50}</math></del> $D_w$	<del><math>5 \times 10^{-4}</math> (Gries: 0.014)</del> Alpine: 0.01; Gries: 0.02	m
<u>Initial till height</u>	<u><math>H_0</math></u>	<u>Alpine:0.05; Gries: 0.0025</u>	m
Till height limit	$H_{lim}$	0.10	m
Till height erosion limit	$H_g$	0.05	m
Gravitational constant	$g$	9.81	$\text{m s}^{-2}$
Density of water	$\rho_w$	1000	$\text{kg m}^{-3}$
Density of ice	$\rho_i$	900	$\text{kg m}^{-3}$
Density of bedrock	$\rho_b$	2650	$\text{kg m}^{-3}$
Bulk density of sediment	$\rho_s$	1500	$\text{kg m}^{-3}$
Erosional exponent	$l_{er}$	<del>2.02</del> <sup>a</sup> 2.02	-
Erosional constant	$k_g$	<del><math>2.7^{-7}</math></del> <sup>a</sup> <del><math>2.7 \times 10^{-7}</math></del>	$\text{m}^{1-l_{er}} \text{s}^{l_{er}-1}$
Seconds per year	$s_{year}$	<del>3.1536</del> <sup>7</sup> <del><math>3.1536 \times 10^7</math></del>	s
Seconds per day	$s_{day}$	86,400	s
Glen's $n$	$n$	3	-
Ice flow rate factor	$A$	$2.4 \times 10^{-24}$	$\text{s Pa}^{-3}$
Mass-balance gradient	$\gamma$	0.00625	$\text{a}^{-1}$
Basal melt rate	$\dot{m}_b$	$7.3 \times 10^{-11}$	$\text{m s}^{-1}$
Sliding rate factor	<del><math>B_s</math></del> $B$	$3.2 \times 10^{-12}$ ; Gries: <del><math>2.05 \times 10^{-11}</math></del>	$\text{MPa m s}^{-1}$
Sliding exponent	$m$	1	-

**Table 3.** Numerical model parameters

Name	Symbol	Value	Units
Solver tolerance (relative)	reltol	$10 \times 10^{-8}$	-
Solver tolerance (absolute)	abstol	$10 \times 10^{-8}$	m
Maximum timestep	dtmax	21600 (6)	s (hr)
Minimum timestep	dtmin	1	s
Edge length ( <del><math>x</math></del> )	<del><math>ds</math></del> $\lambda$		m
<del>Edge length (<math>y</math>)</del> $dh$ -Cell area	$\delta$		m <sup>2</sup>
Sediment connectivity factor	$\Delta\sigma$	<del><math>10^{-3}</math></del> $10^3$	m
Minimum hydraulic diameter	<del><math>D_{h\min}</math></del> $Dh_{\min}$	0.3	m
Number of cells	$n_n$	-	-
Stack	$s_t$	$\vec{n}_n$	-
Receivers	$r_s$	$4 \times n_n$	-
Number of receivers per cell	$n_r$	$\vec{n}_n$	-
Donors	$d_n$	$4 \times n_n$	-
Number of donors per cell	$n_d$	$\vec{n}_n$	-
Weight of each receiver	$w_r$	$4 \times n_n$	-